

**Tight knot spectrum in QCD**Roman V. Buniy,<sup>1,2,\*</sup> Jason Cantarella,<sup>3,2,†</sup> Thomas W. Kephart,<sup>4,2,‡</sup> and Eric J. Rawdon<sup>5,2,§</sup><sup>1</sup>*Chapman University, Schmid College of Science, Orange, California 92866, USA*<sup>2</sup>*Isaac Newton Institute, University of Cambridge, Cambridge CB3 0EH, United Kingdom*<sup>3</sup>*Department of Mathematics, University of Georgia, Athens, Georgia 30602, USA*<sup>4</sup>*Department of Physics and Astronomy, Vanderbilt University, Nashville, Tennessee 37235, USA*<sup>5</sup>*Department of Mathematics, University of St. Thomas, St. Paul, Minnesota 55105, USA*

(Received 15 May 2013; published 26 March 2014)

We model the observed  $J^{++}$  mesonic mass spectrum in terms of energies for tightly knotted and linked chromoelectric QCD flux tubes. The data is fit with one- and two-parameter models. We predict a possible new state at approximately 1190 MeV and a plethora of new states above 1690 MeV.

DOI: [10.1103/PhysRevD.89.054513](https://doi.org/10.1103/PhysRevD.89.054513)

PACS numbers: 11.27.+d, 11.15.Tk

**I. INTRODUCTION**

In 1867 Lord Kelvin suggested [1] that elementary particles can be knots. While his idea of knotted fluid vortices in the aether as fundamental objects of nature was revolutionary for his time, our present experimental knowledge does not agree with this conjecture. Specifically, we now know that knotted fluid vortices are unstable and worse still, the aether does not exist. Nevertheless, the idea is attractive for its simplicity of relating fundamental physical and mathematical objects, and it should not be discarded out of hand before being tested on various other physical systems. One such system where stable knotted configurations may exist is quantum chromodynamics (QCD), the subject of the present study.

Observations from many experiments can be interpreted as signatures of unusual mesonic states, i.e., bosonic hadrons that are not pure  $q\bar{q}$  [2]. Such states can be broadly divided into the following types: (1) hybrids—bound states of quarks and gluons, like  $q\bar{q}G$  with quantum numbers  $J^{PC} = 0^{-+}, 1^{-+}, 1^{--}, 2^{-+}, \dots$ ; (2) exotics—for example, four and six quark states, such as  $qq\bar{q}\bar{q}$  and  $qqq\bar{q}\bar{q}$  with quantum numbers  $J^{PC} = 0^{--}, 0^{+-}, 1^{-+}, 2^{+-}, \dots$ ; (3) glueballs—states with no valence quarks at all, composed of pointlike or collective glue, e.g., string loops à la Nielsen-Olesen [3], or closed flux tubes. [Even though glueballs do not contain valence quarks, there are certainly sea (virtual) quarks within a glueball.] Glueballs are among the most studied and least understood classes of particles in QCD [4]. Lattice calculations, QCD sum rules, electric flux tube models, and constituent glue models lead to a consensus that the lightest valence quark-free state is a glueball with quantum numbers  $J^{++} = 0^{++}$  [5]. On the lattice, usually only a single glueball state below  $\sim 2$  GeV is considered, since all the excitations are expected to be above this

energy [6]; however, a full study of topological operators responsible for knots and links on the lattice is computationally challenging at present and has not yet been carried out. Nevertheless, studying such configurations would be interesting and potentially important for a better understanding of QCD [7].

Although glueballs, and the  $f$  states they are associated with, are one of the most widely discussed problems in hadronic physics, and, while many glueball models have been proposed [8], there is still no consensus of what constitutes a glueball beyond its  $J^{++}$  quantum numbers. Here we take an egalitarian approach. Specifically, we model all  $J^{++}$  mesonic states, i.e., all  $f_J$  and  $f'_J$  states listed by the Particle Data Group (PDG) [2] ( $f$  states, for brevity), as knotted or linked chromoelectric QCD flux tubes [10]. Hence, we will use the term “glueball” loosely as a shorthand for any  $J^{++}$  state in QCD.

Before presenting our model (which is an updated version of [11]) let us first briefly review the history of closed flux tubes in QCD and knotted solitons. Kelvin’s ideas of knots as particles lay dormant for nearly a century, but have been revived in the last forty years. One of the earliest modern attempts to describe elementary particles in terms of knots and links of quantized flux was made in [12]. These objects can be thought of as solitons, and an extensive survey of soliton solutions to various types of quantum field theories, as well as reprints of many classic papers, can be found in [13].

The idea that glueballs and pomerons can be closed string loops goes back to the early days of string theory [14,15] and that glueballs can be closed QCD flux tubes [16] is nearly as old as QCD itself. Early work on closed loop solitons, including closed Nielsen-Olesen vortex loops [17], with respect to glueballs began in the 1970s, and Rasetti and Regge had discussed knotted Nielsen-Olesen vortex loops already in 1975 [18]. A model of toroidal flux tubes in the Copenhagen vacuum was proposed to describe glueballs [19] and a toroidal bag model of glueballs and their excitation spectra was suggested in [20]. A nonlinear

\*roman.buniy@gmail.com

†jason.cantarella@gmail.com

‡tom.kephart@gmail.com

§ericrawdon@gmail.com

$\sigma$  model with toroidal and knot configurations was investigated [21] where it was suggested that similar solitons could exist in liquid crystals,  $^3\text{He}$  or in fundamental theories. Further work along these lines can be found in [22]. An interesting set of dual variables in  $SU(2)$  Yang-Mills theory has been suggested [23], where the large distance limit describes massive solitonic flux tubes which close on themselves in stable knotlike configurations and are natural candidates for describing glueballs. Related work can be found in [24]. In addition, a connection between a generalized Skyrme action and the Yang-Mills action of QCD has been established in [25], where a knot interpretation of glueballs was also suggested.

In 2002, two of us proposed that  $f_J$  states could be modeled by tightly knotted/linked chromoelectric tubes carrying quantized flux where the energy of a knot/link is geometric and proportional to the length of the tubes [11] and gave a one-parameter fit in good agreement with the data. The numerically observed portion of the tight knot spectrum is nondegenerate and the first known degeneracy of the tight link length spectrum occurs at 6 components. We also argued that any systems that supported knotted/linked quantized flux would have this universal energy spectrum up to scaling. For other related work see [26–29].

In 2003 Faddeev *et al.* [30] identified a twisted unknot with the  $f_0(1500)$ , and the  $\eta_L(1410)$  as a parity doublet and they predicted the lightest QCD knot, the trefoil, would be a state in the 6.4 to 6.5 GeV region. Their spectrum is topological with energy proportional to (self-linking number) $^{3/4}$ ; hence, all knots with a fixed self-linking number are degenerate in their model.

The application of knotted flux tubes to a variety of other systems has been proposed, including a condensate of  $^{87}\text{Rb}$  atoms [31] and the neutrino mass spectrum [32]. Linked strings have also been considered in the context of  $Z$  strings [33]. Pairs of unknotted loops and their links have been studied in  $\sigma$  models in [34].

In addition, confining flux and glueballs from the lattice perspective is reviewed in [35] and there is a recent model describing a QCD string as a chain of constituent gluons bound by nearest neighbor interactions [36]. This model has properties seen in lattice QCD, the  $1/N$  expansion and the quark model.

With this overview complete we can proceed with our analysis.

## II. MODEL

In [11] two of us argued how to generalize various classical ideas from plasma physics to a semiclassical model of knotted and linked configurations in QCD. To this end, we first recall that Maxwell’s equations for an ideal plasma imply that flux lines are locked into the plasma flow. This means that if the flux lines are knotted or linked, then the flux line topology is conserved as the flow evolves. A classical consequence of conservation of topology is the

concept of helicity and its conservation in a plasma [37]. Helicity in this context corresponds to the degree of Gaussian linking of QCD flux tubes. Keeping only the helicity fixed, while allowing other topological changes in flux lines, and minimizing the energy leads to the so-called Taylor states [38] in plasma physics. Keeping flux tube topology fixed leads to tight knots [39] in QCD.

The analogy we are drawing between knotted configurations in QCD and flux lines in a Maxwell plasma is only meant for arguing that helicity conservation can stabilize knots and links. The analogy applies more closely to an unconfined quark-gluon plasma, but we nevertheless think it has some merit if not carried too far. The two most important model assumptions (discussed in more detail below) that take us beyond a Maxwell plasma are (i) the tubes carry a single unit of quantized flux, which leads to a uniform tube cross section, (ii) the flux is confined first and then tightly knotted/linked. From these assumptions alone we conclude that the mass spectrum of knots and links is determined completely by their geometry. Solitons that form in a QGP that are then confined, i.e., knotting first and confinement later, would have a different spectrum.

The simplest configuration of linked flux tubes has the form of a Hopf link (denoted  $2_1^2$ ) in which two unknots are linked together in the simplest way such that the Gaussian linking number is one. This is the tight Hopf link, in which fixed diameter  $d$  flux tubes, carrying one flux quantum each, have the shortest total length. The ratio of the total length of the tubes to their diameter  $d$  is invariant for all such tight Hopf links. We define the “knot energy” of the tight configuration  $K$  as its dimensionless length  $l_K$ ,

$$\varepsilon_0(K) = l_K/d,$$

where in this example  $K = 2_1^2$ , so then  $\varepsilon_0(2_1^2) = 2(2\pi d)/d = 4\pi$ . By knot energy, mathematicians generally mean some kind of repulsive electrostatic energy such as O’Hara’s energy [40] or the Freedman-He-Wang [41] “Möbius energy.” Our  $\varepsilon_0(K)$  is called the ropelength of the configuration and the configurations which minimize the ropelength are called “tight” or “ideal” knots [42]; see also [43]. For the Hopf link and a family of other simple links, where the tight configuration is known, see [44]. As expected, for the Hopf link this configuration consists of two linked circles passing through each other’s centers.

The Hopf link is the simplest link, but there is an infinite family of topologically different link types. Many of these configurations have been tabulated by mathematicians [45,46] and there are different topological invariants (such as linking numbers) which distinguish them. However, regardless of which invariants are used to identify the configurations, the “frozen-in field” hypothesis implies that tube topology is conserved. Hence, we conjecture that the ground states of all systems of flux tubes, with any type

of nontrivial linking, are the states with the shortest length tubes.

Similar to linked flux tubes, we also consider self-linked (knotted) flux tubes, where the associated tight knot states and dimensionless knot lengths are analogously defined. The simplest example of a nontrivially knotted flux tube has the form of the trefoil knot  $3_1$ . This configuration has knot energy which has been numerically calculated to be  $\varepsilon_0(3_1) \approx 16.3715$  [47]. Note that there are no known analytic forms for the lengths of any tight knots or links with nonplanar elements.

To begin the description of the model, we consider a high energy hadron-hadron collision in the process of rehadronization, where there are baryons, mesons, and quantized fluxes confined to tubes. If the tubes are open, with quarks and antiquarks at their ends, then they are excited baryon or meson states. Our interest is in closed tubes which can be self-linked (knotted) or linked with each other. As a key part of our model, we identify all the  $f$  states as knotted or linked QCD chromoelectric flux tubes. The topological quantum numbers (or knot/link type of the configuration) are what stabilizes the knotted and linked configurations, so we assume that nontopological (i.e., unknotted/unlinked)  $J^{++}$  closed flux tube configurations are too unstable to have measurable widths. A configuration with tightly knotted or linked flux tubes in the form of the knot or link  $K$  will be called  $f(K)$ . Note that topological invariants in QCD typically require instanton and Chern-Simons terms for their full description [48], but we will not need these subtleties here.

As argued above, nontrivial knotting and linking leads to quasistable generalized minimum energy states. This implies the following theorem.

**Theorem 1.** *For a configuration with a topological charge measured by the knotting or linking of flux tubes of a constant radius (due to quantized flux, and therefore of constant energy or mass per unit length), the generalized minimum energy state is the one that minimizes  $\varepsilon(K)$  and therefore ties the knot or link with the shortest tube.*

Clearly, the minimum energy corresponds to the minimum dimensionless length of tube needed to support the topology. Since the length and energy coincide up to a rescaling, the proof proceeds trivially by inspection. (Note that this proves a quantum analog of Moffatt's 1985 conjecture that higher order linking leads to positive lower bounds on configuration energy.) We will see below that the approximation of a fixed energy per unit length can be improved by an analysis of the effect of a field rearrangement within a bent tube.

We conclude that the quantum case of tight flux tube configurations is much simpler than the corresponding classical case where one minimizes energy with a flux constraint. However, the quantum case suggests that it may be possible to sum or integrate any large number of

flux quanta to get the classical result for the generalized minimum energy of a Gaussian-linked or higher order topological configuration. (Such a result would complete the proof of Moffatt's conjecture for the classical case.) This is a side issue from our main purpose here that will be explored elsewhere.

Let us now proceed with the further description of our phenomenological model, which is similar to the model in [11], but with some minor modifications. Pulling a quark-antiquark ( $q\bar{q}$ ) pair apart in the QCD vacuum, a chromoelectric flux tube forms along a path connecting the quark and antiquark. If the  $q$  is annihilated against the  $\bar{q}$ , or if it is annihilated by a  $\bar{q}$  in another  $q\bar{q}$  pair, where the new  $q$  is in turn annihilated, etc., to close the path, then a closed flux tube containing one flux quantum can form as an unknot or a knot. A flux tube following such a curved path could also, for instance, be due to multiple scattering of the initial  $q\bar{q}$  pair before its mutual annihilation. If the closed tube is a knot, or if it ends up being linked with another closed tube, then such an object has at least one nonzero topological quantum number, and this quantity is what tends to stabilize the tight configuration, which we either identify with one of the observed  $f$  states or use to predict a new state. To allow hadronization to run its course, we assume that the typical time scale needed to reach a tight configuration is shorter than the typical lifetime of the hadron.

Since the publication of [11] in 2003, there has been slow continuous physics progress in the refinement of the  $f$ -states data as summarized by the PDG [2], with smaller error bars from better statistics and a few new states now listed in their summary tables. The change in the  $f$ -state data that affects our model the most is the PDG's realignment of the mass of the  $\sigma$ , formerly called the  $f_0(600)$  and now reassigned as the  $f_0(500)$ . While there has been no new data since 2007, there has been several new reanalyses of compilations of the existing data. The 2010 PDG value of the  $f_0(600)$  mass was reported to be in the range 400–1200 MeV and we previously used  $800 \pm 400$  MeV as our approximation. Now the PDG is reporting a mass range for the  $f_0(500)$  of 400–550 MeV. This is a drastic change since the range has contracted by a factor of 5 and the central value has dropped by over 300 MeV.

Contrary to the rather gradual physics progress, the mathematical knowledge of tight knots has changed dramatically from what was used in [11] to what it is today [52]. In 2003 the lengths of only a handful of tight knots and nonplanar links were known, and some of those only to an accuracy between 5% and 10%. Now we know the complete length spectrum of the first several hundred tight prime knots and nonplanar links with an accuracy that is assumed to be in the 0.1%–1.0% range for most of this spectrum. The lengths of the composite knots have recently appeared [53]. We present new computations covering

TABLE I. Comparison of the glueball mass spectrum and fit energies for  $\epsilon_0(K)$  less than  $\sim 36$ .  $E_1(K)$  and  $E_2(K)$  are for one- and two-parameter high  $f_0(1370)$  fits.

State	Mass	$K^a$	$\epsilon_0(K)^b$	$E_1(K)^c$	$E_2(K)^c$
$f_0(500)$	$475 \pm 75$	$2_1^2$	12.571 <sup>d</sup>	718	850
$f_0(980)$	$990 \pm 20$	$3_1$	16.381	936	1026
		$4_1^2$	20.011	1143	1195
$f_2(1270)$	$1275.1 \pm 1.2$	$2_1^2\#2_1^2$	20.853 <sup>d</sup>	1192	1234
$f_1(1285)$	$1282.1 \pm 0.6$	$4_1$	21.051	1203	1243
$f_0(1370)$	$1350 \pm 150$	$5_1$	23.608	1349	1361
$f_1(1420)$	$1426.4 \pm 0.9$	$2_1^2\#3_1$	24.671	1410	1411
$f_2(1430)$	$\approx 1430$	$5_2$	24.745	1414	1414
$f_0(1500)$	$1505 \pm 6$	$5_1^2$	24.893	1422	1421
$f_1(1510)$	$1518 \pm 5$	$6_3^3$	25.181	1439	1434
$f_2(1525)$	$1525 \pm 5$	$6_1^2$	27.146	1551	1525
$f_2(1565)$	$1562 \pm 13$	$7_7^2$	27.760	1586	1554
$f_2(1640)$	$1639 \pm 6$	$(2_1^2\#2_1^2\#2_1^2)_{kc}$	28.133 <sup>d</sup>	1608	1571
		$2_1^2\#4_1^2$	28.311	1618	1579
		$6_2^2$	28.356	1620	1582
		$6_1$	28.364	1621	1582
		$3_1\#3_1$	28.521	1630	1589
		$6_2$	28.522	1630	1589
		$3_1\#3_{1m}$	28.537	1631	1590
		$2_1^2\#4_1$	28.742	1642	1599
		$7_8^2$	28.886	1651	1606
		$6_1^3$	28.914	1652	1607
		$6_3$	28.929	1653	1608
		$6_2^3$	29.006	1657	1612
		$6_3^2$	29.057	1660	1614
		$(2_1^2\#2_1^2\#2_1^2)_{lc}$	29.133 <sup>d</sup>	1665	1618
$[f_0(1710)]_1$	$[1720 \pm 6]_1$	$8_7^3$	30.297	1731	1672
		$8_{19}$	30.502	1743	1681
		$7_1$	30.715	1755	1691
$[f_0(1710)]_2$	$[1720 \pm 6]_2$	$8_{20}$	31.557	1803	1730
$[f_2(1810)]_1$	$[1815 \pm 12]_1$	$2_1^2\#5_1$	31.908	1823	1746
		$7_3$	31.975	1827	1749
		$8_{15}^2$	32.093	1834	1755
		$7_2$	32.122	1836	1756
		$7_1^2$	32.129	1836	1756
		$7_4$	32.146	1837	1757
		$3_1\#4_1^2$	32.189	1839	1759
		$8_8^3$	32.514	1858	1774
		$7_2^2$	32.520	1858	1775
		$7_4^2$	32.542	1860	1776

<sup>a</sup>Notation  $n_k^l$  means a link of  $l$  components with  $n$  crossings of the  $k$ th type, see, e.g., [62].  $K\#K'$  stands for the connected sum of  $K$  and  $K'$ , and  $(K)_m$  is the mirror image of  $K$ .

<sup>b</sup>All values of the ropelength  $\epsilon_0(K)$  are from [52], except for composite links that were calculated separately but also with Ridgerunner. The dimensionless length convention agrees with [11] and is a factor of 2 smaller than that in [52].

<sup>c</sup> $E_1(K)$  and  $E_2(K)$  are the values of the fitted mass corresponding to the PDG or predicted mass obtained from  $\epsilon_0(K)$  for one- and two-parameter high  $f_0(1370)$  fits, respectively.

<sup>d</sup>Exact value:  $\epsilon_0(2_1^2) = 4\pi$  (Hopf link),  $\epsilon_0(2_1^2\#2_1^2) = 6\pi + 2$  (chain of three links),  $\epsilon_0((2_1^2\#2_1^2\#2_1^2)_{kc}) = 8\pi + 3$  (key chain link with three keys),  $\epsilon_0((2_1^2\#2_1^2\#2_1^2)_{lc}) = 8\pi + 4$  (linear chain link with four links).

the final piece of the puzzle—ropelengths of composite links—for the first time below. The current limitation on knot energies needed for the model is due to the fact that we are dealing with physical knots and links that can be constricted or distorted (see below), thus increasing the errors on the effective lengths. Even with this caveat, we still can advantageously refit the  $J^{++}$  data by comparing it with high accuracy tight knot and link data after adding estimated errors, all of which is collected in Tables I through IV below.

TABLE II. Comparison of the glueball mass spectrum and fit energies for  $\epsilon_0(K)$  less than  $\sim 36$ .  $E_1(K)$  and  $E_2(K)$  are for one- and two-parameter high  $f_0(1370)$  fits.

State	Mass	$K^a$	$\epsilon_0(K)^b$	$E_1(K)^c$	$E_2(K)^c$
		$3_1\#4_1$	32.6361865	1780	
		$7_5$	32.6411865	1780	
		$2_1^2\#5_1^2$	32.6591866	1781	
		$7_3^2$	32.6751867	1782	
		$8_{10}^3$	32.7351871	1785	
		$8_{21}$	32.7711873	1786	
		$7_7$	32.8161875	1788	
		$7_6$	32.8571878	1790	
		$7_5^2$	32.8731878	1791	
		$7_1^3$	32.9111881	1793	
		$2_1^2\#2_1^2\#3_1$	32.9591883	1795	
		$9_{49}^2$	33.0281887	1798	
		$2_1^2\#5_2$	33.0411888	1799	
		$9_{43}^2$	33.1341893	1803	
		$7_6^2$	33.1671895	1805	
		$8_{16}^2$	33.2211898	1807	
$[f_2(1910)]_1$ , $[1903 \pm 9]_1$ , $[f_2(1810)]_2$ $[1815 \pm 12]_2$		$8_9^3$	33.3591906	1813	
		$8_2^4$	33.7111926	1830	
$[f_2(1950)]_1$ $[1944 \pm 12]_1$		$9_{53}^2$	34.0081943	1844	
		$8_1^2$	34.2141955	1853	
		$9_{46}$	34.3191961	1858	
		$9_{50}^2$	34.3501963	1859	
		$9_{61}^2$	34.6891982	1875	
		$9_{42}$	34.7551986	1878	
		$9_{47}^2$	35.0832005	1893	
$[f_2(1910)]_2$ $[1903 \pm 9]_2$		$9_{51}^2$	35.2762016	1902	

<sup>a</sup>Notation  $n_k^l$  means a link of  $l$  components with  $n$  crossings of the  $k$ th type, see, e.g., [62].  $K\#K'$  stands for the connected sum of  $K$  and  $K'$ , and  $(K)_m$  is the mirror image of  $K$ .

<sup>b</sup>All values of the ropelength  $\epsilon_0(K)$  are from [52], except for composite links that were calculated separately but also with Ridgerunner. The dimensionless length convention agrees with [11] and is a factor of 2 smaller than that in [52].

<sup>c</sup> $E_1(K)$  and  $E_2(K)$  are the values of the fitted mass corresponding to the PDG or predicted mass obtained from  $\epsilon_0(K)$  for one- and two-parameter high  $f_0(1370)$  fits, respectively.

<sup>d</sup>Exact values:  $\epsilon_0((2_1^2\#2_1^2\#2_1^2\#2_1^2)_{kc}) = 10\pi + 4$  (key chain link with four keys).

TABLE III. Low  $f_0(1370)$  curvature-corrected fit: Comparison of the glueball mass spectrum and fit energies for  $\varepsilon(K)$  less than  $\sim 32$ .

State	Mass	$K^a$	$\varepsilon(K)^b$	$E_1(K)^c$
$f_0(500)$	$475 \pm 75$	$2_1^2$	11.724	764
$f_0(980)$	$990 \pm 20$	$3_1$	14.943	974
$f_0(1370)$	$1350 \pm 150$	$4_1^2$	18.250	1189
$f_2(1270)$	$1275.1 \pm 1.2$	$4_1$	19.411	1265
$f_1(1285)$	$1282.1 \pm 0.6$	$2_1^2\#2_1^2$	19.556	1274
$f_1(1420)$	$1426.4 \pm 0.9$	$5_1$	21.559	1405
$f_2(1430)$	$\approx 1430$	$2_1^2\#3_1$	22.697	1479
$f_0(1500)$	$1505 \pm 6$	$5_2$	22.779	1484
$f_1(1510)$	$1518 \pm 5$	$5_1^2$	22.866	1490
$f_2'(1525)$	$1525 \pm 5$	$6_3^3$	23.309	1519
$f_2(1565)$	$1562 \pm 13$	$6_1^2$	24.854	1619
$f_2(1640)$	$1639 \pm 6$	$7_7^2$	25.735	1677
		$6_2^2$	25.924	1689
		$6_1$	26.025	1696
		$2_1^2\#4_1^2$	26.046	1697
		$3_1\#3_{1m}$	26.135	1703
		$3_1\#3_1$	26.151	1704
		$6_2$	26.158	1704
$f_0(1710)$	$1720 \pm 6$	$6_1^3$	26.327	1715
		$(2_1^2\#2_1^2\#2_1^2)_{kc}$	26.449	1723
		$2_1^2\#4_1$	26.466	1724
		$6_3$	26.567	1731
		$6_3^2$	26.590	1733
		$7_8^2$	26.720	1741
		$6_2^3$	26.963	1757
		$(2_1^2\#2_1^2\#2_1^2)_{lc}$	27.449	1788
$f_2(1810)$	$1815 \pm 12$	$7_1$	28.018	1826
		$8_7^3$	28.152	1834
		$8_{19}$	28.458	1854
		$7_3$	29.025	1891
		$8_{20}$	29.151	1899
		$7_1^2$	29.231	1905
		$7_2$	29.330	1911
		$2_1^2\#5_1$	29.339	1912
		$7_4$	29.385	1915
		$3_{1m}\#4_1^2$	29.402	1916
		$8_{15}^2$	29.496	1922
		$3_1\#4_1^2$	29.536	1924
		$7_4^2$	29.544	1925

<sup>a</sup>Notation  $n_k^l$  means a link of  $l$  components with  $n$  crossings of  $k$ th type, see, e.g., [62].  $K\#K'$  stands for the connected sum of  $K$  and  $K'$ , and  $(K)_m$  is the mirror image of  $K$ .

<sup>b</sup>All values of the curvature-corrected knot energies  $\varepsilon(K)$  are modified from [52], except for composite links that were calculated separately but also with Ridgerunner. The dimensionless length convention agrees with [11] and is a factor of 2 smaller than that in [52].

<sup>c</sup> $E_1(K)$  is the value of the fitted mass corresponding to the PDG or predicted mass obtained from  $\varepsilon(K)$ .

TABLE IV. Comparison of the glueball mass spectrum and fit energies for  $\varepsilon(K)$  less than  $\sim 32$ .

State	Mass	$K^a$	$\varepsilon(K)^b$	$E_1(K)^c$
		$2_1^2\#2_1^2\#3_{1A}$	29.682	1934
		$3_1\#4_1$	29.790	1941
		$7_5$	29.806	1942
$f_2(1950)$	$1944 \pm 12$	$2_1^2\#5_2$	29.840	1944
		$7_3^2$	29.873	1946
		$7_6$	29.894	1948
		$7_2^2$	29.895	1948
		$2_1^2\#5_{1m}^2$	29.929	1950
		$2_1^2\#5_1^2$	29.952	1952
		$8_8^3$	29.957	1952
		$7_5^2$	30.015	1956
		$8_{21}$	30.017	1956
		$7_7$	30.092	1961
		$7_1^3$	30.112	1962
		$7_6^2$	30.302	1974
		$9_{43}^2$	30.416	1982
		$8_{16}^2$	30.525	1989
		$8_9^3$	30.571	1992
		$8_{10}^3$	30.605	1994
		$2_1^2\#2_1^2\#3_{1B}$	30.611	1995
		$9_{49}^2$	30.839	2009
		$8_2^4$	30.967	2018
		$8_1^2$	31.214	2034
		$8_3^4$	31.473	2051
		$9_{46}$	31.513	2053
		$9_{50}^2$	31.521	2054
		$9_{53}^2$	31.776	2070
		$9_{61}^2$	31.909	2079
		$9_{47}^2$	31.916	2080
		$9_{42}$	31.950	2082

<sup>a</sup>Notation  $n_k^l$  means a link of  $l$  components with  $n$  crossings of  $k$ th type, see, e.g., [62].  $K\#K'$  stands for the connected sum of  $K$  and  $K'$ , and  $(K)_m$  is the mirror image of  $K$ .

<sup>b</sup>All values of the curvature-corrected knot energies  $\varepsilon(K)$  are modified from [52], except for composite links that were calculated separately but also with Ridgerunner. The dimensionless length convention agrees with [11] and is a factor of 2 smaller than that in [52].

<sup>c</sup> $E_1(K)$  is the value of the fitted mass corresponding to the PDG or predicted mass obtained from  $\varepsilon(K)$ .

Let us summarize the model assumptions:

- (1) There is a one-to-one correspondence between  $f$  states and tightly knotted and linked chromoelectric flux tubes.
- (2) The flux is quantized with one flux quantum per tube.
- (3) Knotted and linked flux tubes are stabilized by topological quantum numbers.
- (4) The tube diameter is in the  $\sim 0.1$  fm range. (This corresponds to a string tension of approximately 400 MeV, which agrees with lattice estimates.)

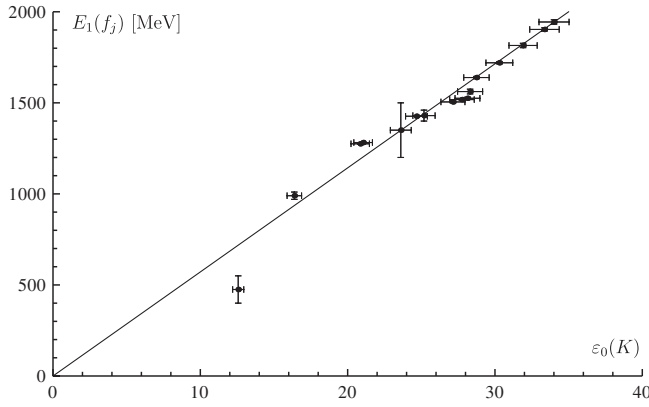


FIG. 1. Fit using uncorrected knot/link lengths: Fit of the  $f_J$  states data to tight knot and link lengths (ropelengths). Errors are shown for the states, but they are too small to be visible for the lengths of tight knots and links, however we include a 3% error in the knot energies due to the fact that we are dealing with physical knots and links. (See discussion in the text.) Nonfitted knots and links are not shown.

- (5) The quantity  $J$  in an  $f_J$  or  $f'_J$  state is the intrinsic angular momentum of the associated knotted solitonic solution of the QCD field equations.
- (6) The relaxation to a tight state configuration (via processes where no topology change is involved) is faster than its decay rate (via processes with topology change) for an  $f$  state, i.e.,  $\tau_{\text{relax}} \ll \tau_{\text{decay}}$ .

One modification from [11] is that we now assume  $J$  is the intrinsic angular momentum rather than the rotational angular momentum. We do this because the tube diameter is now assumed to be smaller and hence the rotational energy level spacing to be larger,  $\sim 500$  MeV, as opposed to a few MeV for the thicker tubes assumed in [11]. The other significant modification is that we correct the energy due to tube curvature as discussed in the next section and include estimated errors due to other physical corrections.

We begin by identifying tight knot and link lengths with glueballs and/or predicted glueballs, where we include all  $f$  states. The lightest candidate is the  $f_0(500)$ , which we identify with the shortest knot or link, i.e., the Hopf link  $2^2_1$ ; the  $f_0(980)$  is identified with the next shortest knot or link, in this case the trefoil knot  $3_1$ , etc.

Our initial one-parameter fit of the data is shown in Fig. 1. The slope is  $\Lambda_{\text{tube}} = 57$  MeV and  $\chi^2 = 84$ . The fit is poor mainly because of the constraint imposed by the very small error bars on the masses of the  $f_2(1270)$  and the  $f_1(1285)$ . We will now see how to improve the fit when ideal tubes are replaced with physical tubes. Note we are already assuming errors of 3% on the knot lengths which anticipates this replacement.

### III. CURVATURE CORRECTIONS

In the discussion so far we have assumed uniform flux across the cross section of the tubes, but flux is not

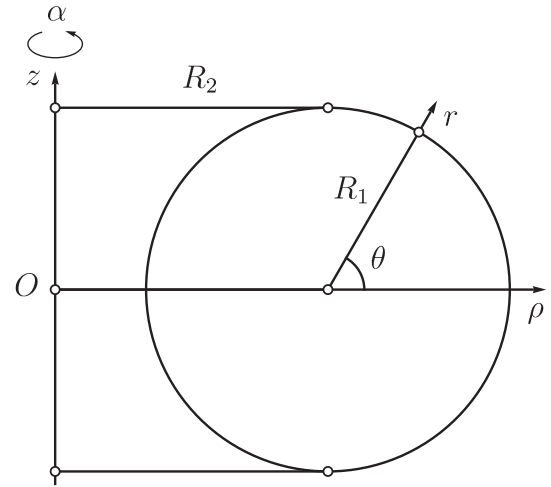


FIG. 2. Cross section of a toroidal flux tube of minor radius  $R_1$  and major radius  $R_2$ . Both polar and cylindrical coordinates are shown.

necessarily uniform over the cross section of curved tubes. This leads us to define a new energy functional for tubes which we call the “flux tube energy.”

To motivate our definition, we consider the effect of bending on the total energy of a field confined to a tube. First, recall that the magnetic field of an ideal toroidal solenoid with fixed flux falls like  $1/\rho$  from the symmetry axis. To see this, choose cylindrical coordinates  $(z, \rho, \alpha)$  as shown in Fig. 2 and note that symmetry requires the field be in the  $\alpha$  direction. (For an elementary argument see [54].) Here we will proceed via a variational argument which is a simpler alternative.

We hold the flux  $\Phi$  fixed and vary the field to find the functional form of the energy  $W$  for a toroidal solenoid. The general form of the energy is

$$W = \frac{1}{2} \int_D B^2 \rho dz d\rho d\alpha. \quad (1)$$

The  $dz d\rho$  integration runs over the cross section of the tube  $D$ . Since  $B$  is independent of  $\alpha$ , the  $\alpha$  integration gives

$$W = \pi \int_D B^2 \rho dz d\rho. \quad (2)$$

The flux through  $D$  is

$$\Phi = \int_D B dz d\rho. \quad (3)$$

Now we want to vary  $W$  with respect to  $B$  while holding  $\Phi$  fixed. This is equivalent to considering

$$\delta(W - \lambda\Phi) = 0, \quad (4)$$

where  $\lambda$  is a Lagrange multiplier. For unit vector  $n$  normal to the cross section, the variation of  $B$  gives

$$\int_D (2\pi B\rho - \lambda n) \cdot \delta B dz d\rho = 0, \quad (5)$$

which vanishes for arbitrary  $\delta B$  only if

$$B(\rho) = \frac{\lambda n}{2\pi\rho}. \quad (6)$$

We find  $\lambda$  from the requirement  $\Phi = \text{const}$ , which gives

$$B = \frac{\Phi}{\rho I}, \quad (7)$$

$$W = \frac{\pi\Phi^2}{I}, \quad (8)$$

with

$$I = \int_D \frac{dz d\rho}{\rho}. \quad (9)$$

To calculate the integral  $I$  over the cross section of a torus of major radius  $R_2$  and minor radius  $R_1$ , it is convenient to introduce polar coordinates  $(r, \theta)$  with the origin at the center of disk  $D$ , plus a toroidal angle  $\alpha$ ; see Fig. 2. The result of integration over  $D$  is

$$I = 2\pi \left[ R_2 - \sqrt{R_2^2 - R_1^2} \right], \quad (10)$$

which leads to

$$W(R_2) = \frac{\Phi^2}{2[R_2 - \sqrt{R_2^2 - R_1^2}]}. \quad (11)$$

The analogous result for the cylinder of length  $2\pi R_2$  is

$$W_0(R_2) = \frac{\Phi^2 R_2}{R_1^2}, \quad (12)$$

and so the ratio

$$\frac{W(R_2)}{W_0(R_2)} = \frac{(R_1/R_2)^2}{2[1 - \sqrt{1 - (R_1/R_2)^2}]}, \quad (13)$$

the graph of which is plotted in Fig. 3, will define our new energy.

Formally, for an embedded tube  $K$  of fixed radius  $R_1$  and parametric centerline curve  $\gamma(s)$  with curvature  $\kappa(s)$ , we define the flux tube energy  $\varepsilon(K)$  by the integral

$$\varepsilon(K) = \frac{1}{2\pi R_1^2} \left( L + \int_0^L \sqrt{1 - R_1^2 \kappa^2(s)} ds \right), \quad (14)$$

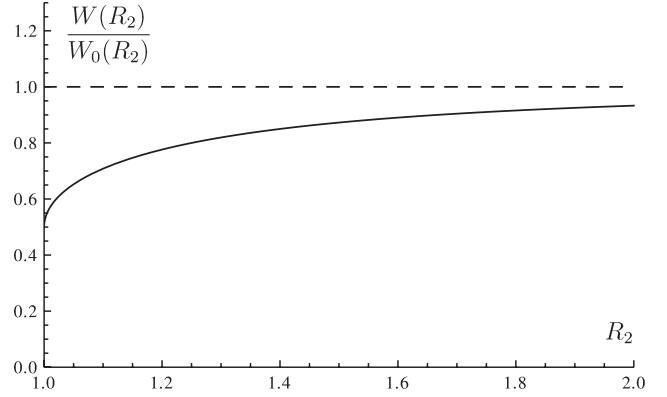


FIG. 3. The function  $W(R_2)/W_0(R_2)$  (solid curve) and its approximation (dashed line) for  $R_2/R_1 \gg 1$  and  $R_1 = 1$ .

where  $L = \int_\gamma ds$  is the length of the center line. [In numerical studies of tight knots and links, it is observed that the integral in (14) is typically  $\sim \frac{\sqrt{3}L}{2}$  which translates into an  $\sim 7\%$  correction of the energy from the ropelength value.] It would be an interesting project to numerically minimize the flux tube energy for various knot and link types. However, this is likely to be a somewhat challenging project: minimizing functionals of curvature (a second derivative of position) constrained by tube contact (a function of position) is quite difficult. Still, there has been recent progress in the numerical modeling of elastic rods with self-contact [55] which leads us to hope that these computations may be tractable in the near future.

In the meantime, we have chosen to minimize the original  $\varepsilon_0(K)$  energy numerically using Ridgerunner [52], and then compute the  $\varepsilon(K)$  energy for the  $\varepsilon_0(K)$ -minimizing configurations on the grounds that the difference between  $\varepsilon(K)$ -minimizing and  $\varepsilon_0(K)$ -minimizing configurations are likely to be small. In Fig. 4 we have histogrammed the shortest 72 knots and links after curvature corrections have been applied. In Fig. 5 we have histogrammed the currently

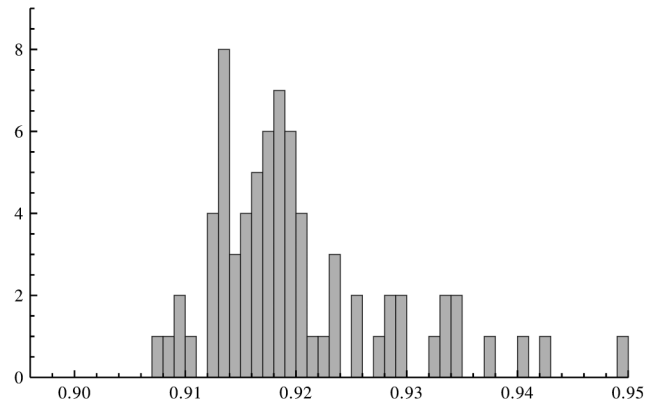


FIG. 4. Histogram of the magnitudes of the curvature corrections to the first 72 knot and link lengths.

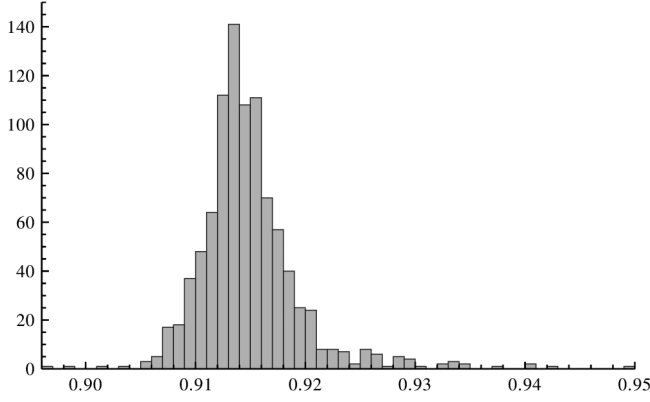


FIG. 5. Histogram of the magnitudes of the curvature corrections to all 945 currently tabulated knot and link lengths.

available complete set of 945 curvature-corrected knots and links.

We should remark that in some cases the curvature is discontinuous, but the field is not. For example, the inner loop of the chain of three elements (the  $2_1^1\#2_1^1$ ) is shaped like a race track—two straight sections connected by two half circles. In a solenoid of this form the curvature is discontinuous at the junctions, but if we move along the field lines we find that the fields are already changing before they reach the junctions since the windings are different in the regions beyond the junction and the field is affected by the fringe fields in that region. Hence the fields can be continuous through the junction.

As an example of a case with both length and curvature corrections that can be calculated exactly [44], consider the chain of three unknots  $2_1^2\#2_1^2$  which has length  $6\pi + 2 \approx 20.8496$  and has  $R_2 = 2R_1$  in curved regions and  $R_2 \rightarrow \infty$  in straight sections. We find an overall corrected value

$$\begin{aligned} \varepsilon(2_1^2\#2_1^2) &= \frac{1}{4(2-\sqrt{3})} (6\pi + 2) \approx 0.933013(6\pi + 2) \\ &\approx 19.4529. \end{aligned} \quad (15)$$

Note that all exactly calculable link lengths in our tables are unique, but degeneracies can occur at longer lengths. The first such examples are the links corresponding to the  $E_6$  and  $D_6$  Dynkin diagrams. Both have the length  $\varepsilon_0(E_6) = \varepsilon_0(D_6) = 12\pi + 7$  (which falls slightly beyond the largest lengths included in our tables) and both have the same curvature-corrected energy  $\varepsilon(E_6) = \varepsilon(D_6) = \frac{3\pi}{(2-\sqrt{3})} + 7$ . Other corrections should lift this degeneracy.

#### IV. RESULTS

In our model, the chromoelectric fields [56]  $F_{0i}$  are confined to the knotted and linked tubes, each carrying one quantum of conserved flux [57,58]. We consider a stationary Lagrangian density

$$\mathcal{L} = \frac{1}{2} \text{tr} F_{0i} F^{0i} - V, \quad (16)$$

where, similar to the MIT bag model [59], we included the possibility of a constant energy density  $V$ . To account for conservation of the flux  $\Phi_E$ , we add to  $\mathcal{L}$  the term

$$\text{tr} \lambda [\Phi_E / (\pi a^2) - n^i F_{0i}], \quad (17)$$

where  $n^i$  is the normal vector to a section of the tube of radius  $a$  and  $\lambda$  is a Lagrange multiplier. Varying the full Lagrangian with respect to  $A_\mu$ , we find

$$D^0(F_{0i} - \lambda n_i) = 0, \quad (18)$$

$$D^i(F_{0i} - \lambda n_i) = 0, \quad (19)$$

which have the constant field solution

$$F_{0i} = (\Phi_E / \pi a^2) n_i. \quad (20)$$

With this solution, the energy is positive and, to first approximation, proportional to the length of the tube  $l$  and thus the minimum of the energy is achieved by shortening  $l$  (i.e., tightening the knot), subject to the curvature correction discussed above and other corrections discussed below.

We proceed to identify knotted and linked QCD flux tubes, i.e., curvature-corrected physical flux tubes, with glueballs and/or predicted glueballs, where we include all  $f$  states. The lightest candidate is the  $f_0(500)$ , which we identify with the shortest curvature-corrected knot or link, i.e., the Hopf link  $2_1^2$ ; the  $f_0(980)$  is identified with the next shortest knot or link, in this case the trefoil knot  $3_1$ , etc. By the fourth knot/link, the ordering begins to be reshuffled due to the curvature corrections, see Tables I and III.

All knot and link lengths have been calculated for states corresponding to energies well beyond 2 GeV. Above  $\sim 2$  GeV the number of knots and links grows rapidly, and so the corresponding hadronic states should become dense relative to their typical width. Hence we will confine our investigations to knot lengths corresponding to all known  $f$  states below  $\sim 2$  GeV.

Our detailed results are collected in Table I through IV, where we list the masses and error bars for the  $f$  states (other properties can be found in [2]) and our identifications of these states with knots and links together with the corresponding knot and link lengths (see Tables I and II), curvature-corrected lengths (see Tables III, IV, and V), and fitted energies.

We will give two interpretations of the data. The first possibility is with the  $f_0(1370)$  identified with the  $5_1$  knot which results in a prediction of a new state near 1190 MeV identified with the  $4_1^2$  link. The other possibility, which gives our best fit, is to identify the  $f(1370)$  itself with

TABLE V. High  $f_0(1370)$  curvature-corrected fit: Comparison of the glueball mass spectrum and fit energies for  $\varepsilon(K)$  less than  $\sim 32$ . Except for the  $f(4_1^2)$ , this table contains only the fitted PDG states. Predictions for other states can be gotten by multiplying the knot energy by the appropriate value of  $\Lambda_{\text{tube}}$ .

State	Mass	$K$	$\varepsilon(K)$	$E_1(K)$
$f_0(500)$	$475 \pm 75$	$2_1^2$	11.724	763
$f_0(980)$	$990 \pm 20$	$3_1$	14.943	972
$f(4_1^2)$		$4_1^2$	18.250	1187
$f_2(1270)$	$1275.1 \pm 1.2$	$4_1$	19.411	1263
$f_1(1285)$	$1282.1 \pm 0.6$	$2_1^2 \# 2_1^2$	19.556	1272
$f_1(1420)$	$1426.4 \pm 0.9$	$5_1$	21.559	1403
$f_0(1500)$	$1505 \pm 6$	$2_1^2 \# 3_1$	22.697	1477
$f_2(1430)$	$\approx 1430$	$5_2$	22.779	1482
$f_1(1510)$	$1518 \pm 5$	$5_1^2$	22.866	1488
$f_2'(1525)$	$1525 \pm 5$	$6_3^3$	23.309	1516
$f_2(1565)$	$1562 \pm 13$	$6_1^2$	24.854	1617
$f_2(1640)$	$1639 \pm 6$	$7_2^2$	25.735	1674
$f_0(1370)$	$1350 \pm 150$	$6_2^2$	25.924	1687
$f_0(1710)$	$1720 \pm 6$	$(2_1^2 \# 2_1^2 \# 2_1^2)_{\text{kc}}$	26.449	1721
$f_2(1810)$	$1815 \pm 12$	$7_1$	28.018	1823
$f_2(1910)$	$1903 \pm 9$	$7_2$	29.330	1908
$f_2(1950)$	$1944 \pm 12$	$2_1^2 \# 5_2$	29.840	1941

the  $4_1^2$  link to give a one-to-one matching of the first 12  $f_J$  states with the first 12 knots and links. We will discuss the details of these options below.

For comparison purposes we have displayed results for knot energies proportional to lengths (Tables I and II) and also for the curvature-corrected knot energies, (see Tables III, IV and V). Let us begin with the uncorrected length case. In Fig. 1 we display a one-parameter least-squares fit to the experimental data (below 1945 MeV) for the mass spectrum of  $f$  states identified with knots and links. The fit is

$$E(K) = \Lambda_{\text{tube}} \varepsilon_0(K), \quad \Lambda_{\text{tube}} = 57.14 \pm 0.53 \text{ MeV}, \quad (21)$$

where  $\varepsilon_0(K)$  is the dimensionless length of the knot or link  $K$  as defined above. The fit (21) shows fair agreement with our model. One measure of the quality of the fit is given by the adjusted  $R$  squared,  $R^2 = 0.998$ . Since we have more knots than  $f$  states, the relevance of  $R^2$  must be carefully interpreted and not taken at face value, especially beyond  $\sim 1700$  MeV where the lack of particle data per knot becomes pronounced.

Compared to our 2003 results [11], the  $f_0(500)$  now falls well below the line of our fit and we pay a penalty in  $\chi^2$ . The result is also partially responsible for the change in the value of our fit parameter  $\Lambda_{\text{tube}}$ , compared to what we find using the 2010 values for the  $f_0(600)$ . It will be interesting to see if the new  $f_0(500)$  PDG numbers are stable. Since they are extracted from partial wave analysis and multiply subtracted dispersion relations, there are questions about

comparing with the mass values for other  $f$  states found in invariant mass plots. There is also the important issue of mixing with four quark and other resonances. However, we are not in a position to comment further on these matters with confidence except for the general qualitative remark that in a flux tube model we could expect mixing with excited mesons if there is resonant behavior of tube breaking (forming a  $q\bar{q}$  pair) and rejoining (by annihilating the pair). Resonant breaking and rejoining at two positions, or in two link tubes mixes with four quark states, etc.

Next we consider the curvature-corrected case where the one-parameter fit is shown in Fig. 6. The  $\chi^2$  is substantially improved over the uncorrected length case and drops to  $\chi^2 = 33$  to a large extent due to the fact that the two most restricting states, the  $f(1270)$  and the  $f(1285)$ , have been brought in line with the rest of the  $f_J$  data by the curvature corrections. Hence, we continue to consider only the curvature-corrected length case for the remainder of this section.

Figure 7 shows the locations of knots and links with no corresponding  $f$  state; hence, it gives the locations of new states predicted by the model. Our first new state is at 1190 MeV, corresponding to the  $4_1^2$  link. It is interesting to consider the PDG entry for the state  $f_2(1270)$ . Of the 36 quoted experimental observations, all but one is within three  $\sigma$  of the PDG average mass of 1275 MeV. The  $5.5\sigma$  outlier at  $(1220 \pm 10)$  MeV is from the process  $pp \rightarrow pp\pi^+\pi^-$  in the experiment of Breakstone *et al.* [60], and we suggest its identification with our predicted state at  $\sim 1190$  MeV.

We further predict twelve states around  $(1710 \pm 20)$  MeV. To justify such a proposal, one only needs to look at the PDG entry for the state  $f_0(1710)$  to see a considerable amount of tension in the data with a large number of incompatible mass measurements in this region. We interpret this

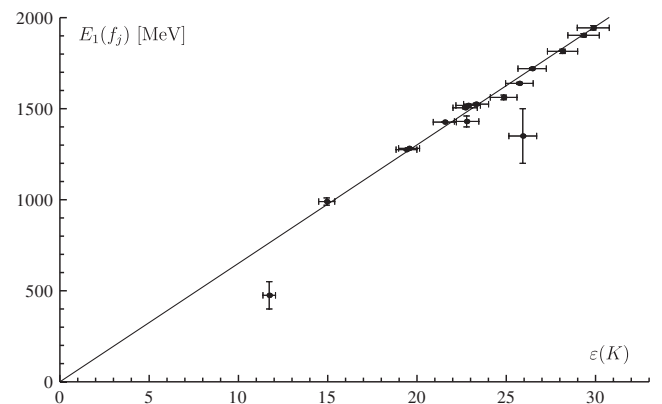


FIG. 6. Fit using curvature-corrected lengths: High one-parameter  $f_0(1370)$  fit of the  $f_J$  states data to the curvature-corrected knot and link data. Errors are shown for the states, and the 3% estimated from the text is shown for the knots and links. Nonfitted knots and links are not shown in this figure.

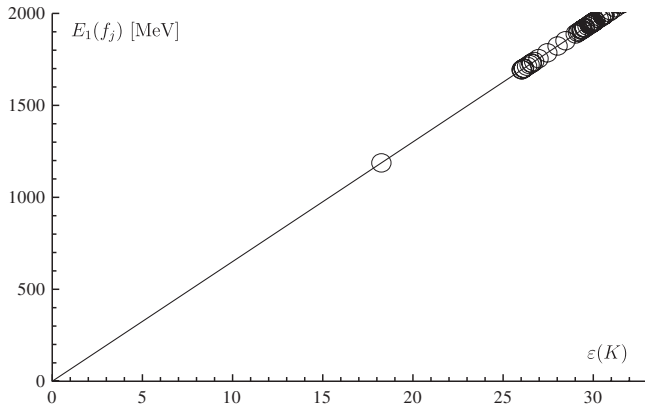


FIG. 7. Predictions using curvature-corrected lengths: The circles are locations of knots and links that do not have corresponding  $f_J$  states in Fig. 6. Hence these are the locations of states predicted by the high  $f_0(1370)$  one-parameter fit of the model.

as an indication of multiple  $J^{++}$  states near 1700 MeV that need to be resolved, just as is suggested by our model; see Tables I and III. Similar reasoning applies to the states in the vicinity of  $f_2(1810)$ ,  $f_0(1910)$ , and  $f_2(1950)$  where there is also tension in the data. A global statistical analysis of  $f$ -state data to establish a statistical significance of such an interpretation should be carried out. Figure 8 gives both the combined fit and predicted masses and is displayed for convenience. Better HEP data will provide further tests of the model and improve the high mass identification.

Even though the states become denser with energy, they also become more and more difficult to produce, wider and therefore less stable. We expect the production cross section to depend on how complicated a knot/link is. This is a somewhat vague statement, because to make it precise one would need to know the probability of formation of a configuration with certain values of the knot and link invariants. While there has been some work on knot formation [61], these are for random stick knots and so application

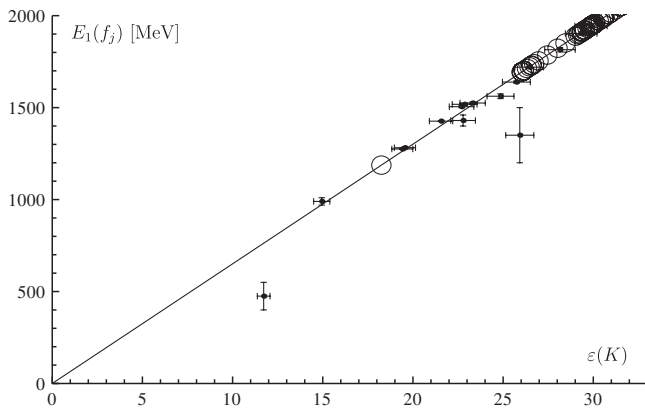


FIG. 8. Curvature-corrected lengths: The combined set of measured and fitted states (dots with error bars) and predicted states (circles) for the high  $f_0(1370)$  one-parameter fit.

to QCD is premature. If calculations of this type could be carried out in QCD, then they should provide guidance for the production of favored versus disfavored knot/link types. Once one has a set of favored production states, then one could go on to predict the spectrum that would be visible above some cross-section limit, and this would be less dense than the spectrum predicted in the manuscript. It could also explain why some of the states we predict have not been seen—their production cross section is too low in experiments carried out to date, or they could also be too wide to have been seen. (The calculation of decay widths of knots and links is also an open problem as will be discussed at length below.) As a general rule we would expect more massive states to be wider and more difficult to produce. Such results could provide guidance to experiments as they would provide a set of effective selection rules.

We are now ready to discuss the second fit possibility. Since the error on the  $f_0(1370)$  mass is rather large ( $\pm 150$  MeV) it can be identified with several different knots and links. However, the identifications of the other  $f$  states, except for the  $f_0(500)$ , are much more constrained due to the small errors on their masses and this in turn restricts the identification of the  $f_0(1370)$  to two allowed choices with reasonable  $\chi^2$ s. We call the case discussed above the high fit, where we identify the  $f_0(1370)$  with the  $5_1$  knot, and the low fit where we identify the  $f_0(1370)$  with the  $4_1^2$  link. The high fit is the one that predicts a new state at  $\sim 1190$  MeV, while the low fit gives a one-to-one match between the first 12  $f$  states and the first 12 knots and links. The low fit gives a somewhat better  $\chi^2$ , but the high fit gives an acceptable  $\chi^2$  and could be required if for instance the 1220 MeV state of [60] is confirmed, making it necessary to free up a low energy knot/link to identify with it. Since we have already presented the high fit above, we now proceed to discuss the low fit.

The low fit leaves no gaps in the spectrum until we get near 1700 MeV. See Figs. 9, 10, and 11. The  $\chi^2$  is improved and the fitted value of  $\Lambda_{\text{tube}}$  is similar to the high-fit case. We find

$$E(K) = \Lambda_{\text{tube}}\epsilon(K), \quad \Lambda_{\text{tube}} = 65.16 \pm 0.61 \text{ MeV}. \quad (22)$$

The low fit (22) is our best overall fit to the data. We have tabulated the fitted energies for the first 72 knots and links, identifying all  $f$  states of energy less than 2 GeV, hence giving predictions of many new states at 1690 MeV and above.

Now let us discuss the statistical significance of our results. First, we have done a number of tests to determine if our hypothesis that glueballs are knotted flux tubes is likely to be correct. Let us begin with the well-known Kolmogorov-Smirnov test, which tests distribution functions  $\hat{F}(y)$  and  $F(y)$  by means of the quantity

$$\sup_y |\hat{F}(y) - F(y)|,$$

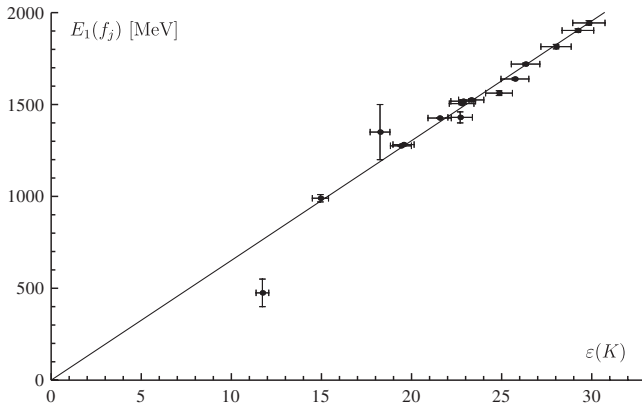


FIG. 9. Low  $f_0(1370)$  one-parameter fit with curvature-corrected lengths: This is our best fit of the  $f_J$  states data to the knot and link data. Errors are shown for the states, as is the 3% error estimate of knot and link lengths. Nonfitted knots and links are not shown.

which in this case are the distribution functions of the glueball masses and calculated knot and link lengths. The resulting  $p$  value for the Kolmogorov-Smirnov test is

$$p_{\text{KS}} = 0.95, \quad (23)$$

where we recall that  $p$  is bounded  $0 \leq p \leq 1$  and  $p < 0.01$  implies poor correlation,  $0.01 < p < 0.05$  implies moderate correlation, and  $0.1 < p$  implies strong correlation. Hence, the Kolmogorov-Smirnov test implies our model is in excellent agreement with the data.

The Kolmogorov-Smirnov test is a measure of goodness of fit. We summarize this and a number of other goodness-of-fit tests as well as several variance tests in Table VI. All show excellent agreement between model and data. Here and below we give  $p$  values for the high-fit case. The low-fit values are similar.

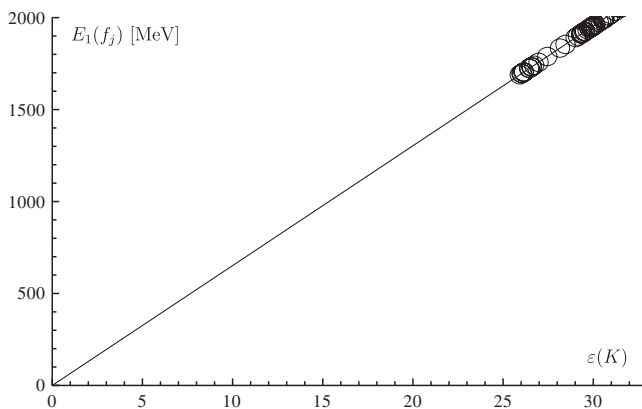


FIG. 10. Low  $f_0(1370)$  one-parameter fit for curvature-corrected lengths: This figure shows the knots and links that do not have corresponding  $f_J$  states in Fig. 9. Hence these are the locations of states predicted by the model.

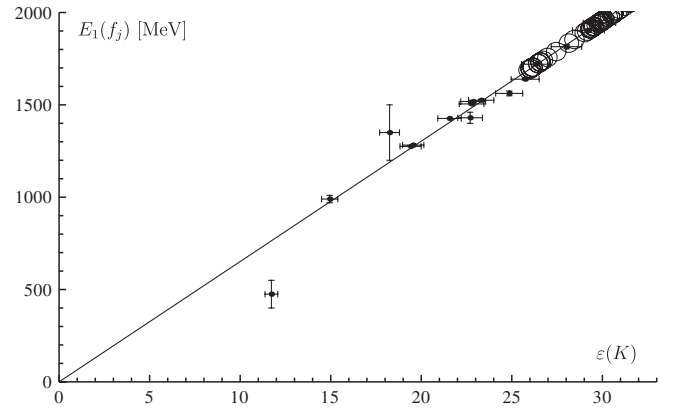


FIG. 11. Low  $f_0(1370)$  one-parameter fit for curvature-corrected lengths: This figure shows the combined set of measured and fitted states (dots with error bars) and predicted states (circles).

Another approach is to calculate the  $\chi^2$  for the data set, subject to the corrections of energy per unit length differences and deformations from the ideal knot case. We have argued that the minimum energy and minimum length of knots do not necessarily coincide. While we expect the average energy per unit length of a knot does not strongly depend on knot type, there is still a small correction due to this effect. In addition, the tubes can be constricted due to being wrapped by another section of the tube or distorted by wrapping tightly around another section of tube (as a rope wrapped tightly around a post). We can approximate such corrections and will consider a typical example below.

We have calculated the change in energy of a pair of linked flux tubes to provide an example of corrections we should expect due to constriction, which in turn gives a contribution to the expected error in using physical tubes instead of tight mathematical tubes to model glueballs. The example we consider is a cylindrical tube along the  $z$  axis encircled by a toroidal tube lying in the  $xy$  plane at  $z = 0$ . We assume both tubes have a circular cross section with that of the torus staying fixed, but that of the cylinder being of reduced radius in the region of constriction,

TABLE VI. Statistical tests of the model. Recalling that  $p$  is bounded  $0 \leq p \leq 1$  and  $p < 0.01$  implies poor correlation,  $0.01 < p < 0.05$  implies moderate correlation, and  $0.1 < p$  implies strong correlation, we see that all these tests strongly support the model.

Goodness-of-fit test	$p$ value	Variance test	$p$ value
Pearson $\chi^2$	0.66	Brown-Forsythe	0.74
Kolmogorov-Smirnov	0.95	Fisher Ratio	0.69
Cramér-von Mises	0.96	Levene	0.74
Anderson-Darling	0.97	Siegel-Tukey	0.82
Kuiper	0.99		
Watson U Square	0.90		

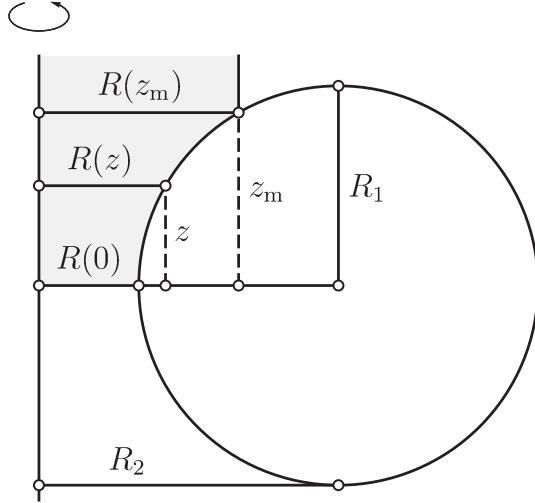


FIG. 12. Cross section of a toroidal flux tube of minor radius  $R_1$  and major radius  $R_2$  constricting a cylindrical flux tube of radius  $R(z)$ .

$$R(z) = R(0) + R_1 - (R_1^2 - z^2)^{1/2}, \quad (24)$$

where

$$-z_m \leq z \leq z_m, \quad z_m = [R_1^2 - R^2(0)]^{1/2}; \quad (25)$$

see Fig 12. We further assume both tubes carry the same amount of flux and so set their undistorted radii equal,  $R_1 = R(z_m)$ . The torus would tighten until  $R_2 = R_1$ , except that it begins to encounter the cylindrical tube at  $R_2 = 2R_1$ . The torus energy

$$\Delta W_1 = W(R_2) - W(2R_1), \quad (26)$$

where the function  $W$  is defined in (3), falls as it tightens and the energy in the cylindrical tube

$$\Delta W_2 = \frac{\Phi_2^2}{\pi} \left[ -\frac{z_m}{R_2^2} + \int_0^{z_m} \frac{dz}{R^2(z)} \right] \quad (27)$$

grows as it is constricted. Stability is reached by minimizing  $\Delta W_1 + \Delta W_2$  with respect to  $R(0)$ ; see Fig. 12.

We have estimated the constriction for the Hopf link of two magnetic flux tubes and find a  $\sim 30\%$  correction over the region of constriction, which translates into an overall  $\sim 5\%$  correction to the link energy, since about 15% of the Hopf link is constricted. We expect distortion effects to be similar. However, since all knots and links have similar corrections that modify their total energies in the same direction, we expect the spread in variation to be smaller than the correction itself. Hence a  $\delta \sim 5\%$  error on physical knot energies versus tight knot energies is not unreasonable. An actual QCD flux tube could be more rigid due to confinement effects, so we can justify reducing the error bars to something smaller. Even assuming QCD flux tubes

are substantially more rigid than magnetic flux tubes, we still find an acceptable value for  $\chi^2$ . For example, letting  $\delta_{\text{QCD}} = 3\%$  we find the model is in reasonable agreement with the data as seen in the figures for the fits.

In terms of the bag model [59], the interiors of flux tubes of tight knots correspond to the interiors of bags. The flux in the tube is supported by current sheets on the bag boundary (surface of the tube). Knot complexity can be reduced (or increased) by unknotting (knotting) operations [62,63]. In terms of flux tubes, these moves are equivalent to reconnection events [64]. Hence, a metastable glueball may decay via reconnection. Once all topological charge is lost, metastability is lost, and the decay proceeds to completion. Two other glueball decay processes are flux tube or string breaking [65–67] (this favors large decay widths for configurations with long flux tube components) and quantum fluctuations that unlink flux tubes (this would tend to broaden states with short flux tube components).

Since the publication of [11], some minor quantitative progress has been made in understanding knot flux tube decay, but these results are still insufficient to go beyond the qualitative observations made in [11]. However, we pause here to discuss the present state of our understanding of the decay of knots and links in order to clarify why progress is difficult. We discuss the three processes in order:

- (1) Tube breaking: First consider tube breaking. When a tube carrying a single flux quantum breaks, a section of the tube disappears and is replaced by a  $q\bar{q}$  pair. To calculate this process, one begins by following Schwinger's classical analysis of  $e^+e^-$  pair production in a strong electric field, but now instead of an infinite region of field we have a cylindrical region and backreaction must be included. For a straight tube, solutions involve parabolic cylinder functions and Airy functions, but for most of the cases of interest we have bent tubes, so we need curvature corrections. Thus, to calculate the tube breaking for a typical knot, we must integrate corrected local breaking over the full length of the tube in the knot. So far we have partial analytic results for the straight tube case. The full calculation is challenging, and will take a considerable amount of numerical work to extend it to the full knot/link spectrum.
- (2) Tunneling: Another path to decay is via quantum tunneling. Consider a tight Hopf link where the tubes lie at right angles to each other. The tubes touch along intersecting rings that run along their inner radii. The tunneling takes place most efficiently along the line that connects their centers of mass (other paths are exponentially suppressed). The calculation is complicated by the fact that extended objects are tunneling, not particles as can be assumed in examples like nuclei decay. Knots will be even more difficult to deal with as their contact surfaces are

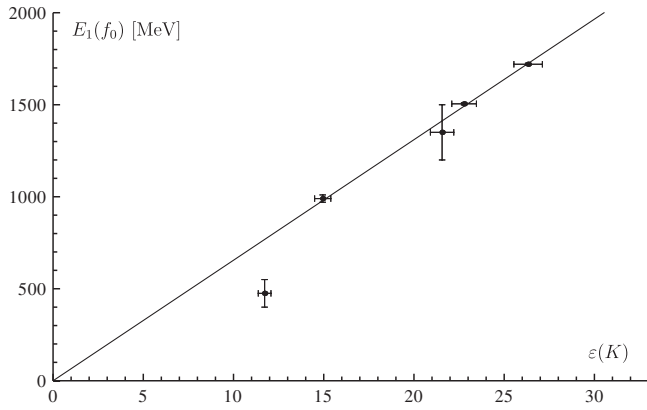


FIG. 13. The  $f_0$  states data is fitted to the curvature-corrected knot and link data. Errors are shown for the states and estimated to be 3% for the knot/link energy. Nonfitted knots and links are not shown.

complicated, and the tubes touch at a variety of angles. In this case one would need to integrate over the contact surface with proper weighting to take angular effects into account. At present we are still far from having reliable estimates of tunneling rates.

- (3) Reconnection: Reconnection decays appear to be more complicated than either string breaking or tunneling, since reconnection involves one or more strings breaking with  $q\bar{q}$  pair production, then rearrangement of the tube positions and then finally tube reconnection via  $q\bar{q}$  pair annihilation. Again, this must be integrated over the knot. Hence we believe it is necessary to fully understand string breaking and aspects of production via  $q\bar{q}$  annihilation before significant progress can be achieved on the realistic reconnection calculations of flux tubes.

Let us make one final comment about the model. A more conservative approach is to assume only the  $0^{++}$  states, i.e., the  $f_0$  states, correspond to knotted/linked flux tubes. In that case there are only five states to fit and the result is displayed in Fig. 13 for comparison, where the identified states are

$$[f_0(500), f_0(980), f_0(1370), f_0(1500), f_0(1710)] \leftrightarrow [2_1^2, 3_1, 5_1, 5_2, 6_2]. \quad (28)$$

The predicted states in this case are shown in Fig. 14. The slope is essentially unchanged, the  $R^2 = 0.998$  value is roughly the same. The masses of the predicted states can be easily gotten by rescaling the knot lengths in the table with the new slope parameter  $\Lambda_{\text{tube}} = (65.50 \pm 1.81)$  MeV. Note that the  $f_0(1370)$  has been moved in the ordering to improve the fit. More data is needed to distinguish between the fit of all  $f_J$  states and the restricted  $f_0$  fit.

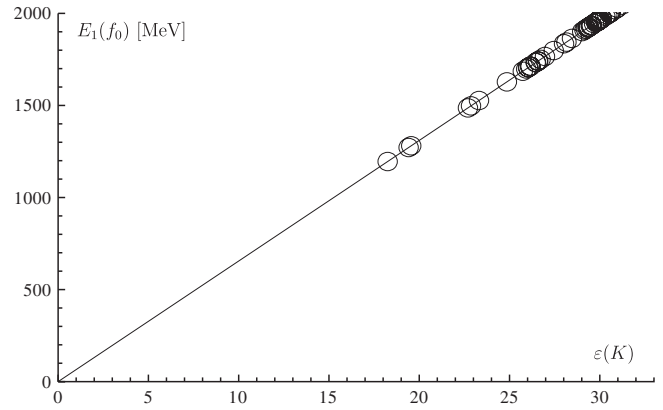


FIG. 14. The  $f_0$  states data is fitted to the curvature-corrected knot and link data and only the predicted states (circles) are shown.

The  $\chi^2 = 15.62$  for the fit is not particularly good but it only takes replacing the new  $f_0(500)$  values with the old  $f_0(500)$  mass and error bars to get  $\chi^2 = 0.56$ . So if the new  $f_0(500)$  mass is due to mixing and one could extract the unmixed value for the pure gluonic state it is possible that the fit would improve again.

If a sufficient number of  $f_J$  states are found, so that they outnumber the total number of knots and links, then this would be evidence to support the restricted fit (since all short knots and links are presumed to be known). However, this is not the case at present.

## V. DISCUSSIONS AND CONCLUSIONS

We have considered hadronic collisions that produce some number of baryons and mesons plus a gluonic state in the form of a closed QCD flux tube (or a set of tubes). From an initial state, the fields in the flux tubes quickly relax to an equilibrium configuration, which is topologically equivalent to the initial state. (We assume topological quantum numbers are conserved during this rapid process.) The tube radius is set by the confinement scale, so to lowest order the energy of the final state depends only on the topology of the initial state and equals the length  $l_K$  of the tube times the average energy per unit length, or the dimensionless knot or link length  $\epsilon_0(K)$  times the energy scale parameter  $\Lambda_{\text{tube}}$ . While related to  $\Lambda_{\text{QCD}}$  by constants of order unity,  $\Lambda_{\text{tube}}$  can be more accurately determined (see above) and hence could be a useful dimensional parameter in studying other properties of QCD, such as scattering and hadronization processes. The relaxation proceeds through the minimization of the field energy. This process occurs via shrinking the tube length and the process halts to form a tight knot or link. Flux conservation and energy minimization also force the fields to be homogeneous across the tube cross sections for straight tube sections and the fields fall like  $1/\rho$  for curved sections as shown above. We have estimated corrections to the simple energy-length

proportionality and have used them to correct and place error bars on the physical knot lengths.

Details of knot excitations would be interesting to investigate, as would other quantum corrections, but at present we do not have a reliable way to estimate these effects, nor do we have a good way to calculate glueball decay rates. However, we do expect high mass glueball production to be suppressed because more complicated nontrivial topological field configurations are statistically disfavored and we also expect higher mass glueballs to be relatively less stable.

On the lattice the glueball is associated with a plaquette operator that, when operating on the vacuum, creates a closed loop of chromoelectric flux [68]. This loop is a path on a square lattice and the glueball mass should be proportional to the length of the path. Using our assumption that topologically trivial paths are too unstable to allow measurable masses and assuming that we are studying single flux tubes on the lattice (no links), the first stable closed loop on the lattice will be the trefoil. The shortest length for a trefoil on a square lattice is 24 lattice spacings (24 tube diameters in dimensionless units), so, without smoothing, the lattice should predict the lightest glueball mass to be a factor of  $24/\varepsilon(3_1)$  larger than the value we quote in the table, i.e.,

$$E_{\text{lattice}}(3_1) \sim \frac{24}{\varepsilon(3_1)} E(3_1) \sim 1450 \text{ MeV}. \quad (29)$$

While this naive result is only a rough approximation, it could be refined and does indicate that lattice calculations of glueball masses can come out on the high side. It is also an explanation of why our results differ from lattice predictions.

In addition to not fitting naturally into the quark model [69], glueballs have some other characteristic signatures, including enhanced production via gluon rich channels in the central rapidity region, branching fractions incompatible with  $q\bar{q}$  decay, very weak coupling to  $\gamma\gamma$ , and Okubo-Zweig-Iizuka suppression. All the  $f$  states have some or all of these properties. For instance, none have substantial branching fractions to  $\gamma\gamma$ . However, mixing with  $q\bar{q}$  isoscalar states can obscure some of these properties. All these observations are in qualitative agreement with the model presented here.

Our high-fit model predicts one new state at 1190 MeV, twelve states concentrated near 1700 MeV, and a tower of higher mass states with the next dense concentration starting near 1900 MeV. The low-fit model makes similar prediction except that there is no new state near 1200 MeV. We have argued that there is sufficient tension in the experimental data in these regions to allow the identification of many more states with knots and links. A careful statistical analysis of the data of all  $f$  regions to resolve hidden states is needed. Recall we are assuming that  $J$  is intrinsic angular

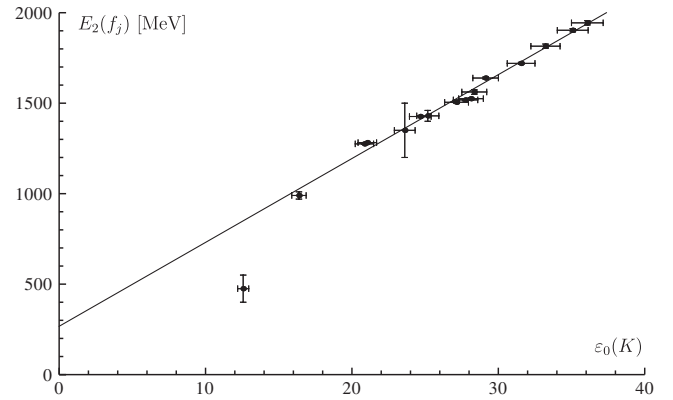


FIG. 15. Uncorrected lengths: Two-parameter fit of the  $f_J$  states data to the knot and link data. Errors are shown for the states, but they are too small to be visible for the knots and links. However, a 3% knot length error is included for reasons discussed in the text. Nonfitted knots and links are not shown.

momentum and not rotational angular momentum as we assumed in [11].

As a variant example of the models we have been considering and as a comparison, we consider a two-parameter fit to the  $f_J$  data where the origin is not fixed at zero glueball mass and zero tube length. Fitting the non-curvature-corrected length data to the glueball data gives a shallower slope and an intercept at positive glueball mass; see Fig. 15. While the  $\chi^2$  is somewhat better than for the non-curvature-corrected one-parameter fit, we do not have an interpretation of the nonzero intercept other than a zero length tubular bag constant which seems rather unphysical. This problem does not arise for either the high- or low-fit two-parameter models with curvature-corrected lengths. As seen in Figs. 16 and 17 the intercepts in both these models are consistent with zero. This result and in addition to the improved  $\chi^2$  when we use the curvature-corrected knot lengths in the

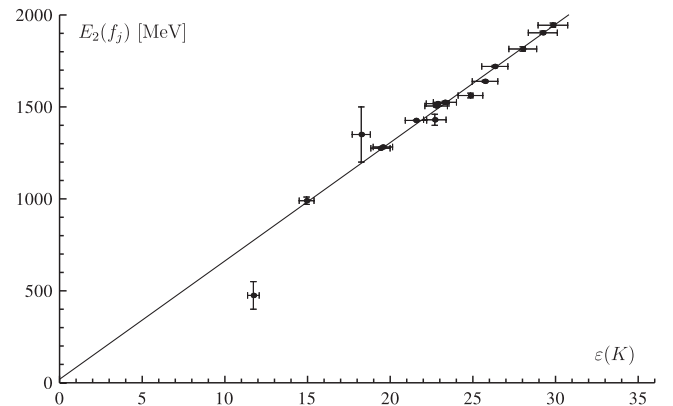


FIG. 16. Two-parameter fit with curvature-corrected length: Two-parameter low  $f_0(1370)$  fit of the  $f_J$  states data to the knot and link data. Errors are shown for the  $f$  states, and a 3% error is estimated for knot and link lengths. Nonfitted knots and links are not shown.

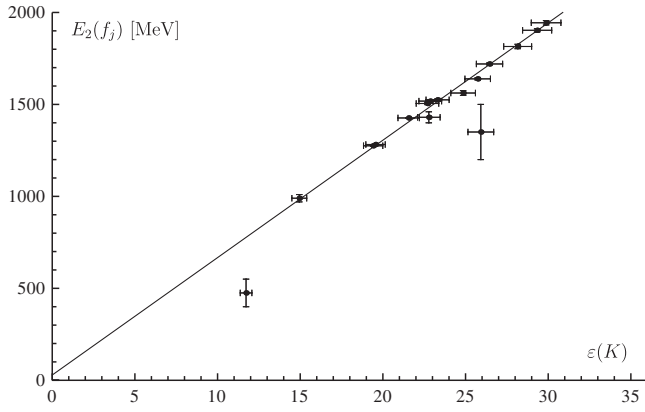


FIG. 17. Two-parameter fit with curvature-corrected length: Two-parameter high  $f_0(1370)$  fit of the  $f_j$  states data to the knot and link data. Errors are shown for the  $f$  states and estimated for the knots and links. Nonfitted knots and links are not shown.

one-parameter fits gives us confidence that either our one-parameter (i.e., the slope  $\Lambda_{\text{tube}}$ ) high or one-parameter low curvature-corrected fits are the sufficient and best choices for a robust model.

We note that some of the states can be degenerate at lowest order due to the symmetries of some knots and links. The trefoil comes in two versions, left and right handed, and there are two Hopf links, one with linking number  $+1$  and one with linking number  $-1$ . Some prime knots have a  $\mathbb{Z}_2 \times \mathbb{Z}_2$  symmetry leading to a potential fourfold degeneracy. The cases of links and composites are even more complicated, with a variety of higher degeneracies possible [70]. How these degeneracies can be lifted at higher order is a topic for future research, but let us make a few comments here. Since many knots and links come in more than one form, we can consider their mixings. For example, the trefoil can be left handed  $3_1^L$  or right handed  $3_1^R$ . Since the trefoil can decay by changing a single crossing, changing two crossings can take  $3_1^L$  to  $3_1^R$ . We have identified the  $3_1$  with  $f_0(980)$  whose width is  $\sim 50$  MeV. Assuming the decay is via reconnection or quantum tunneling, then we expect the  $3_1^L$  and  $3_1^R$  versions to mix at the  $10^{-3}$  level by changing two crossings. This corresponds to a  $\sim 1$  MeV level splitting and is undetected experimentally. As the quantum state  $\psi_{3_1} = \frac{1}{\sqrt{2}}(3_1^L - 3_1^R)$  has self-linking number  $SL(\psi_{3_1}) = 1$  when properly normalized, while  $\psi'_{3_1} = \frac{1}{\sqrt{2}}(3_1^L + 3_1^R)$  has  $SL(\psi'^{3_1}) = 0$ , we would expect the  $\psi'_{3_1}$  to be the more stable linear combination,

and the proper state to be identified with the  $f_0(980)$ . Similar comments apply to all our identifications. Note that the Hopf link comes in only one form, so it corresponds to the single broad state  $f_0(500)$ . Mixing could potentially be detected for other broad states where splitting could be a few MeV, but only when they are identified with knots or links that come in more than one type.

It would be trivial to extend our predictions to states above 2 GeV. One just takes the knot of appropriate lengths from [52] and scales them by the dimensionful parameter  $\Lambda_{\text{tube}}$  from the fit. However, there is insufficient mesonic data above 2 GeV to improve or constrain our fit. More experimental data to test the model in this region would be very welcome.

Knotted and linked magnetic fields configurations have been discussed with respect to a number of plasma phenomena including spheromaks [71], astrophysical [72] and atmospheric [73] objects. Similar comments apply to Bose-Einstein condensates [74] and various field theories. The system we consider is intrinsically different since we assume that in QCD we have confinement into tubes and then the tubes get knotted and linked, as opposed to finding knotted or linked fields that then may or may not get confined. In our case we expect energy proportional to tube length (with corrections as discussed in this paper), where the later case not involving initial confinement would not necessarily be expected to have a simple length-energy relationship. The energies and sizes of these classical solitons are sometimes difficult to quantify since they depend on parameters of the plasma, including temperature, pressure, density, ionic content, etc. However, it was argued in [11] that well-defined topological soliton energies can be identified for vacuum QCD or any vacuum quantum-flux-tube system. Hence we emphasize that in all systems which support quantum flux tubes, including those occurring in media, from the quark-gluon plasma to superconductors, the energy spectrum of knot and link solitons will be universal up to a scaling for fixed values of parameters [76,75].

To conclude, we have given two interpretations of the  $f$ -state data with a model of knotted chromoelectric flux tubes in QCD. The first possibility is where the  $f(1370)$  is identified with the  $5_1$  knot which results in a prediction of a new state around 1190 MeV which is identified with the  $4_1^2$  link. The other possibility—which also gives our best fit—is to identify the  $f(1370)$  with the  $4_1^2$  link to give

TABLE VII. Fit parameters for the model at 95% C.L. We collect the results for the various choices of one- and two parameter fits so raw length fits can be compared with curvature-corrected fits.

Fitting parameter	1p-length	2p-length	1p-cc-high	2p-cc-high	1p-cc-low	2p-cc-low
$\chi^2$	83.9	45.4	33.3	33.1	28.3	28.4
$\Lambda_{\text{tube}}$	$57.14 \pm 0.53$	$46.36 \pm 2.64$	$65.06 \pm 0.61$	$63.83 \pm 3.57$	$65.16 \pm 0.61$	$64.34 \pm 3.59$
Intercept	0	$267.11 \pm 69.55$	0	$28.74 \pm 82.18$	0	$19.16 \pm 82.51$
$R^2$	0.998	0.967	0.999	0.977	0.999	0.980

a one-to-one matching of all the first twelve  $f_J$  states with the first twelve knots and links. We have collected the results for the various choices of one- and two parameter fits in Table VII. Experiments could help to resolve which of these two possibilities is the correct choice.

Finally, we should point out that there is a considerable amount of tension in the  $f_J$  data, as indicated by the  $\chi^2$ s of the individual states quoted by the PDG. We would not expect our fits to be better than the fits of the data on which they are based.

### ACKNOWLEDGMENTS

We have benefited from discussions and email correspondences with many colleagues over the last several years. We especially thank James Bjorken, Hai-Yang Cheng, and Ryan Rohm for useful comments. We also thank the Isaac Newton Institute for hospitality while this work was being completed. The work of T. W. K. was supported by U.S. DoE Grant No. DE-FG05-85ER40226, and DE11328 that of E. J. R. by NSF DMS #1115722. Many of the knot and link lengths were calculated using Vanderbilt's Advanced Computing Center for Research and Education (ACCRE). We thank Tom DeGrand and David Lin for discussions [7], and we thank A. Niemi for pointing out Ref. [9].

*Note added in proof.*—Recently, we have become aware of two related works. First, thin flux tubes have recently shown up in another context. Bjorken *et al.* [77] have recently used aligned thin flux tube scattering to explain the correlations between particles with the similar azimuthal angle seen by the CMS Collaboration in very high-multiplicity  $pp$  collisions [78,79]. In addition, Todorova [80,81] has argued that a natural length scale of  $68 \pm 2$  MeV arises when one studies the late stages of hadronization in the context where QCD strings have acquired a helical structure as suggested by Andersson *et al.* [82]. This scale is remarkably close to our value  $\Lambda_{\text{tube}} = 65.16 \pm 0.61$  MeV and we hope to explore the possible relationship in the future.

### APPENDIX

The understanding of the spectrum of hadrons began with the quark model, which already had a long history before the advent of QCD. String theory has its origins in the attempt to understand strong interaction scattering processes. Now it is clear that QCD is the correct theory of the strong force, but this theory is notoriously difficult to solve because it is strongly coupled at a large distance, complicating the low energy region. However, it was realized in the 1970s that a lattice approximation can, in principle, go a long way in allowing us to obtain results in the strong coupling region of the theory. Furthermore, one can start with a lattice QCD Lagrangian and derive a combined quark model and flux tube theory from first principles,

which contains the relevant properties of the old quark model plus the stringlike behavior of flux tubes. There is a vast amount of literature on this subject. The models that were first studied in the nonrelativistic limit have subsequently been extended to the relativistic case. Many corrections have been included, and our understanding of the spectrum and interactions have improved enormously over the years. However, issues remain. Our model is an attempt to make sense of a controversial part of the hadronic spectrum. There have been many states identified with glueballs—i.e., states without valence quarks. Sometimes they are modeled as closed flux tubes, sometimes as bound states of gluons. Our model focuses on extending the nonrelativistic tube sector of the full relativistic tube plus the quark theory derived from QCD. We can form metastable states from knotting or linking tubes if we assume they carry quantized flux and that all topological quantum numbers are conserved to lowest order, as magnetic helicity is for an ideal plasma as mentioned above. We emphasize that these states are formed from first confining flux into tubes and then knotting them, not in the reverse order. The ordering with confining first gives the spectrum we derive, while knotting first gives a solitonic spectrum more like one would expect in plasma physics. For QCD, knotting without confinement could apply to states in the quark-gluon plasma, but we will not discuss that issue here.

The quark model has its origins in the study of current algebra and symmetry principles in the early 1960s. Important discussions and early papers and reviews can be found in the reprint volumes by Gell-Mann and Ne'eman [83] and Kokkedee [84]. As experimental data had been collected, the quark model evolved and it was realized that a good approximation of the hadronic spectrum can be obtained from simple potential models.

Our purpose in this appendix is to review enough of the history of the quark plus tube model to place our extension of that model in context. Many of the general approaches of early works on quark potentials and tubes are still valid today.

Our philosophy is perhaps closest to Isgur and Paton's flux tube model [85,86] circa 1985, which they derived heuristically from lattice QCD. At small length scales (the weak coupling limit), they argue that the degrees of freedom are the quarks and gluons, while at large distances (strong coupling) the degrees of freedom become quarks and tubes. Confinement is automatic in their model, as they discuss. While we are focused on closed tubes, we suppose it is part of the full strong coupling theory. That means we fully agree with standard quark model results, but as in Isgur and Paton, the naive quark model receives corrections from the tube sector, e.g., a heavy  $q\bar{q}$  pair connected by an unexcited tube is a ground state meson. Exciting d.o.f. of the tube turns this state into a hybrid (a bound state of  $q\bar{q}$  and a gluon from the weak coupling perspective, which is not a good approximation here).

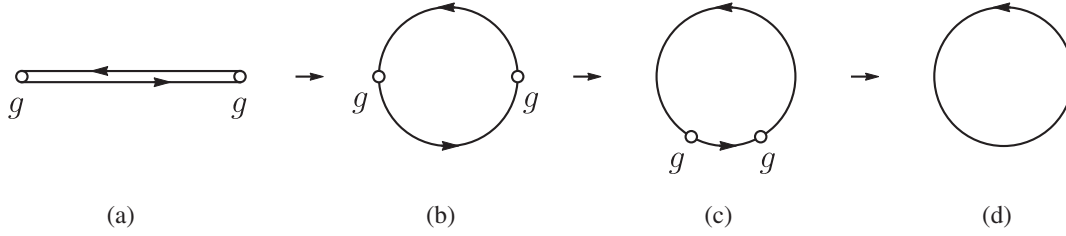


FIG. 18. Gluon bound state-closed tube complementarity: (a) Gluon pair bound by a color adjoint (octet) tube, (b) gluon pair bound by a pair of fundamental color (triplet) tubes, (c) gluons can move along the triplet tubes, (d) gluons have annihilated to form a closed triplet tube.

Gluon-tube duality: If we consider a glueball as a bound state of gluons in the tube model (we will limit ourselves to two gluons for this discussion), then between them is a gluonic tube carrying the octet color [see Fig. 18]. We can think of this tube as being composed of a pair of fundamental triplet color tubes. Let us assume that the stable configuration is when the octet splits to this pair, as the Casimir invariant analysis suggests; see Fig. 18. Consideration of the stability of an octet tube is analogous to the difference between type I and type II superconductors. In type I, multiquanta flux tubes are stable, while in type II they split into unit quantum flux tubes. QCD multi-flux tubes are known to be near the stability boundary. Now let the gluons move together [see Fig. 18] on the tube and annihilate. (See [87], [88] and [89] for related discussions.) We are left with a closed fundamental loop of quantized flux in Fig. 18. From our arguments in the text, a single unknot of this type is unstable, but knotting the loop or linking a pair of loops gives the configuration chromoelectric helicity, and would tend to stabilize it.

This plasma analogy was included in the Introduction to demonstrate that topologically conserved quantities can play a part in stabilizing flux configurations, but it does not capture other important properties of QCD-like confinement. Whether QCD flux tubes behave as type I or type II superconductors, the fact remains that if the QCD phase transition has either superconducting property, then it is likely to have some properties similar to an ideal plasma and to satisfy helicity conservation at the classical level, with violations coming from quantum processes like tunneling.

Let us return to the bound gluon pair case. Simple potential models were introduced to study  $gg$  bound states already by the early 1980s, although it was controversial whether to treat the gluon as a massless [90] or a massive particle [91–93], and this affected the degree of freedom counting. However, both interpretations attributed an effective mass to the gluon due to confinement.

A potential of the form [90]

$$V_0(r) = -\frac{3\alpha_s}{r} + a_g r \quad (\text{A1})$$

was used for the massless gluon case, where  $\alpha_s$  is the coupling strength from light quark potential models, and  $a_g$  is

the coefficient (Regge slope) of the long-range force, i.e., the linear potential between the gluons. For the massive case, the string part of the potential can be written [91]

$$V_s(r) = -2m(1 - e^{-r/r_0}), \quad (\text{A2})$$

where  $m$  is the effective mass of the gluon, and the scale  $r_0$  is set by the slope  $a_g = \frac{2m}{r_0}$ . Solving the Schrödinger equation with these potentials led to predictions of the low-lying states.

As mentioned above, Isgur and Paton [85,86] developed a rather complete quark and tube model from lattice QCD, and studied potentials of the form

$$V_0^q(r) = -\frac{4\alpha_s}{3r} + c + br \quad (\text{A3})$$

for quarks that can be regulated at the origin by including an additional term to give the full quark potential

$$V^q = V_0^q(r) + \frac{\pi}{r}(1 - e^{-f\sqrt{b}r}), \quad (\text{A4})$$

where the parameter  $f$  provides the cutoff. Here  $c$  is an effective bag constant, and the strong coupling is allowed to run with  $r$ .

For gluons a similar form was studied

$$V^g = 2\pi br + c' + \frac{\gamma}{r}(1 - e^{-f'\sqrt{b}r}), \quad (\text{A5})$$

where  $\gamma$  and  $f'$  are parameters. Notably, they take  $c' = 0$  in their analysis of low-lying states, which corresponds to the absence of a bag constant in the gluonic potential. Three gluon bound states were also studied in detail in [94,95].

Including relativistic effects improves the results of the quark model [96,97]. Schrödinger equation potential models were replaced with the spinless Salpeter equation [98,99]. Semirelativistic and relativistic models [100] with  $KE = \sqrt{\mathbf{p}^2 + m^2}$  have continued to be studied with stunning results for mesons and suggestive results for glueballs [101,102]. Other more field-theoretic approaches to the low-lying glueball spectrum have been studied in the literature [103,104], but we will not discuss them here since our model is more akin to the potential models.

An instructive full group-theoretic accounting of bound states of two, three, and four gluons can be found in [105]. Single gluons bound to a static color source (gluelumps) are also considered there. The conclusion is that  $0^{++}$  and  $2^{++}$  are the lowest lying states, as expected. Given this result and the bound gluon-closed tube duality mentioned above justifies our identification of  $f_J$  states with closed tubes. There are three  $f_1$  states in our analysis, and we assume they have intrinsic spin = 1. If these three states are not identified with knots/links, then we would predict three more  $J$  even states at these locations.

Returning to the specifics of our model, we are considering only long (relative to their radius) closed tubes in their ground state, so to a good approximation, we need only the linear part of the potential. Taking

$$V = c' + a_g r, \quad (\text{A6})$$

we then fit the  $f_J$  states as in the text and find  $c'$  consistent with zero, which agrees with the assumption in [86], for the glueball case, and the slope parameter found by the fit in the text. Our main new feature is that we fix a set of relative lengths by the tight knot/link assumption, and then have one parameter  $a_g$  (or  $\Lambda_{\text{tube}}$  in the text) with which to fit the data. Our results and model are fully compatible with the relativistic quark model, but we are only interested in the nonrelativistic sector, since the knots are not excited in our discussion. (We also have additional assumptions

TABLE VIII. Relevant quantum field theory operators.

$J^{PC}$	Operators
$0^{++}$	$\mathbf{E}_a^2 \pm \mathbf{B}_a^2 \rightarrow \mathbf{E}_a^2$
$2^{++}$	$E_a^i E_a^j \pm B_a^i B_a^j - \frac{1}{3} \delta^{ij} (\mathbf{E}_a^2 \pm \mathbf{B}_a^2) \rightarrow$ $E_a^i E_a^j - \frac{1}{3} \delta^{ij} \mathbf{E}_a^2$

beyond those of the standard relativistic quark-tube model.) However, we could consider such excitations, and then the full relativistic model would come into play. Finally, let us mention that from a quantum field theory perspective, the operators we are most interested in are displayed in Table VIII and they correspond to the energy stored in chromoelectric fields, if we ignore confining bag energy. But it should be kept in mind that these are local operators and to capture the nonlocal knot/link information we need to integrate them over the closed tube length. In the present work we have extended this analysis to curvature-corrected lengths as described in the text.

What is new in our model is that tight knots and links have not previously been studied in potential models, nor have they been analyzed in lattice QCD. We hope our work will inspire the lattice community to consider such an undertaking, since we believe they could study the stability of knots and links by keeping track of topological invariance of configurations as they step through a simulation.

- 
- [1] Sir William Thomson (Lord Kelvin), Proc. R. Soc. Edinburgh, Sect. A **VI**, 94 (1867).
- [2] K. Nakamura *et al.* (Particle Data Group), *J. Phys. G* **37**, 075021 (2010).
- [3] H. B. Nielsen and P. Olesen, *Nucl. Phys.* **B61**, 45 (1973).
- [4] E. S. Swanson, *AIP Conf. Proc.* **432**, 471 (1998).
- [5] For further discussion of glueballs and their quantum numbers see, for instance, G. B. West, *Nucl. Phys. B, Proc. Suppl.* **54**, 353 (1997); N. A. Tornqvist, [arXiv:hep-ph/9510256](https://arxiv.org/abs/hep-ph/9510256); J. Terning, [arXiv:hep-ph/0204012](https://arxiv.org/abs/hep-ph/0204012); R. C. Brower, *Int. J. Mod. Phys. A* **16**, 1005 (2001); M. Suzuki, *Phys. Rev. D* **65**, 097507 (2002); M. Teper, *Nucl. Phys. B, Proc. Suppl.* **109**, 134 (2002).
- [6] C. J. Morningstar and M. J. Peardon, *Phys. Rev. D* **60**, 034509 (1999).
- [7] A general study of knotted flux tubes on the lattice has yet to be performed and would be quite difficult.
- [8] Many of the  $f$  states have been discussed as possible glueball states or as states expected to have some glueball content. The favored states have changed over the years, but without definitive clarification. For instance, a recent paper [9] focuses on the glueball nature of the  $f_0(600)$  but also discusses the gluonic content of numerous other  $f$  states and contains numerous references. The history of glueball models is long and complicated, and so we refer the reader to the literature.
- [9] G. Mennessier, S. Narison, and W. Ochs, *Phys. Lett. B* **665**, 205 (2008).
- [10] Confinement is due to monopole condensation in terms of the 't Hooft's dual confinement picture, with flux tubes being chromoelectric. However, since we as yet have no soliton solutions to the full QCD theory, all we require are tightly knotted/linked flux tubes (chromoelectric, chromomagnetic, or even chromodyonic) of a uniform cross section, though we prefer to go with conventional interpretation.
- [11] R. V. Buniy and T. W. Kephart, *Phys. Lett. B* **576**, 127 (2003).
- [12] H. Jehle, *Phys. Rev. D* **3**, 306 (1971); *Phys. Rev. D* **6**, 441 (1972); *Phys. Rev. D* **11** 2147 (1975); *Phys. Lett.* **104B** 203 (1981); *Phys. Lett.* **104B** 207 (1981).
- [13] *Solitons and Particles*, edited by C. Rebbi and G. Soliani (World Scientific, Singapore, 1984).
- [14] J. Scherk, *Rev. Mod. Phys.* **47**, 123 (1975).
- [15] G. Bhanot and C. Rebbi, *Nucl. Phys.* **B180**, 469 (1981).
- [16] See, for example, the discussion by G. 't Hooft, *Nucl. Phys.* **B190**, 455 (1981).

- [17] H. J. de Vega, *Phys. Rev. D* **18**, 2945 (1978).
- [18] M. Rasetti and T. Regge, *Physica (Amsterdam)* **80A**, 217 (1975).
- [19] B. S. Skagerstam and A. Stern, *Phys. Lett.* **97B**, 405 (1980).
- [20] D. Robson, *Z. Phys. C* **3**, 199 (1980).
- [21] L. D. Faddeev and A. J. Niemi, *Nature (London)* **387**, 58 (1997).
- [22] L. D. Faddeev and A. J. Niemi, arXiv:hep-th/9705176; J. Gladikowski and M. Hellmund, *Phys. Rev. D* **56**, 5194 (1997); R. A. Battye and P. M. Sutcliffe, *Phys. Rev. Lett.* **81**, 4798 (1998); R. A. Battye and P. Sutcliffe, *Proc. R. Soc. A* **455**, 4305 (1999).
- [23] L. D. Faddeev and A. J. Niemi, *Phys. Rev. Lett.* **82**, 1624 (1999).
- [24] T. R. Govindarajan, *Mod. Phys. Lett. A* **13**, 3179 (1998); S. V. Shabanov, *Phys. Lett. B* **458**, 322 (1999); P. van Baal and A. Wipf, *Phys. Lett. B* **515**, 181 (2001).
- [25] Y. M. Cho, *Phys. Rev. Lett.* **87**, 252001 (2001).
- [26] A. Wereszczynski and M. Slusarczyk, *Eur. Phys. J. C* **30**, 537 (2003).
- [27] A. P. Protogenov, *Phys. Usp.* **49**, 667 (2006).
- [28] D. Jia and Y.-P. Lu, arXiv:1108.5887.
- [29] M. Kobayashi and M. Nitta, *Phys. Lett. B* **728**, 314 (2014).
- [30] L. Faddeev, A. J. Niemi, and U. Wiedner, *Phys. Rev. D* **70**, 114033 (2004).
- [31] Y. M. Cho, *Int. J. Pure Appl. Phys.* **1**, 246 (2005).
- [32] T. W. Kephart, P. Leser, and H. Pas, *Mod. Phys. Lett. A* **27**, 1250224 (2012).
- [33] J. Garriga and T. Vachaspati, *Nucl. Phys. B* **438**, 161 (1995); T. W. Kephart, *Phys. Rev. D* **58**, 107704 (1998).
- [34] R. S. Ward, *Phys. Lett. B* **473**, 291 (2000); J. Hietarinta and P. Salo, *Phys. Lett. B* **451**, 60 (1999).
- [35] J. Kuti, *Nucl. Phys. B, Proc. Suppl.* **73**, 72 (1999).
- [36] J. Greensite and C. B. Thorn, *J. High Energy Phys.* **02** (2002) 014.
- [37] L. Woltier, *Proc. Natl. Acad. Sci. U.S.A.* **44**, 489 (1958); H. K. Moffatt, *J. Fluid Mech.* **35**, 117 (1969); *J. Fluid Mech.* **159** 359 (1985).
- [38] J. B. Taylor, *Phys. Rev. Lett.* **33**, 1139 (1974).
- [39] V. Katritch, J. Bednar, D. Michoud, R. G. Scharein, J. Dubochet, and A. Stasiak, *Nature (London)* **384**, 142 (1996); O. Gonzalez and J. H. Maddocks, *Proc. Natl. Acad. Sci. U.S.A.* **96**, 4769 (1999); P. Pieranski and S. Przybyl, *Phys. Rev. E* **64**, 031801 (2001); A. Stasiak, J. Dubochet, V. Katritch, and P. Pieranski, *Ideal Knots and their Relation to the Physics of Real Knots* (World Scientific, Singapore, 1998), p. 1.
- [40] J. O'Hara, *Topol. Appl.* **48**, 147 (1992).
- [41] M. H. Freedman, Z.-X. He, and Z. Wang, *Ann. Math.* **139**, 1 (1994).
- [42] R. A. Litherland, J. Simon, O. Durumeric, and E. J. Rawdon, *Topol. Appl.* **91**, 233 (1999); O. Gonzalez, and J. H. Maddocks, *Proc. Natl. Acad. Sci. U.S.A.* **96**, 4769 (1999); A. Nabutovsky, *Commun. Pure Appl. Math.* **48**, 381 (1995).
- [43] F. Maggioni and R. L. Ricca, *Proc. R. Soc. A* **465**, 2761 (2009).
- [44] J. Cantarella, R. B. Kusner, and J. M. Sullivan, *Inventiones Mathematicae* **150**, 257 (2002).
- [45] H. Doll and J. Hoste, *Math. Comput.* **57**, 747 (1991).
- [46] J. Hoste and M. B. Thistlethwaite, and J. R. Weeks, *Math. Intelligencer* **20**, 33 (1998).
- [47] P. Pieranski and S. Przybyl, "High Resolution Portrait of the Ideal Trefoil Knot," (to be published).
- [48] See [49] for recent results on the instanton or the lack thereof in the QCD vacuum, and [50] and [51] for a study of knots and Chern-Simons terms in gauge theories.
- [49] H. B. Thacker, *Proc. Sci., LATTICE2008* (2008) 260.
- [50] E. Witten, *Nucl. Phys.* **B149**, 285 (1979).
- [51] E. Witten, *Commun. Math. Phys.* **121**, 351 (1989).
- [52] T. Ashton, J. Cantarella, M. Piatek, and E. J. Rawdon, *Exp. Math.* **20**, 57, (2011).
- [53] J. Cantarella, A. LaPointe, and E. J. Rawdon, *J. Phys. A* **45**, 225202 (2012).
- [54] D. J. Griffiths, *Introduction to Electrodynamics* (Benjamin Cummings Press, San Francisco, 1999), 3rd. ed.
- [55] M. Chamekh, S. Mani-Aouadi, and M. Moakher, *Comput. Methods Appl. Mech. Eng.* **198**, 3751 (2009); J. Spillmann and M. Teschner, *Eurographics* **27**, 497 (2008).
- [56] To describe chromomagnetic flux tubes, we use the Lagrangian density  $\mathcal{L} = \frac{1}{2} \text{tr} F_{ij} F^{ij} - V$  to which we add  $\text{tr} \lambda \{ \Phi_B / (\pi a^2) - \frac{1}{2} \epsilon^{ijk} n_i F_{jk} \}$ . Then the variation gives  $D^j (F_{ij} - \frac{1}{2} \epsilon_{ijk} n^k \lambda) = 0$  with resulting constant fields  $F_{ij} = (\Phi_B / \pi a^2) \epsilon_{ijk} n^k$ . Again, the energy is positive and proportional to  $l$ .
- [57] In a discussion of flux quantization in non-Abelian gauge theories, it is important to keep the following fact in mind. For a static configuration, and using the temporal gauge, we can avoid the creation of chromomagnetic flux lines inside the flux tubes [3]. A dual argument shows chromoelectric flux creation can be avoided as well.
- [58] For other approaches to solitonic bags see R. Friedberg and T. D. Lee, *Phys. Rev. D* **18**, 2623 (1978); R. Goldflam and L. Willets, *Phys. Rev. D* **25**, 1951 (1982); G. Clement and J. Stern, *Phys. Rev. D* **34**, 1581 (1986).
- [59] A. Chodos, R. L. Jaffe, K. Johnson, C. B. Thorn, and V. F. Weisskopf, *Phys. Rev. D* **9**, 3471 (1974); T. DeGrand, R. L. Jaffe, K. Johnson, and J. E. Kiskis, *Phys. Rev. D* **12**, 2060 (1975); A. Chodos, R. L. Jaffe, K. Johnson, C. B. Thorn, and V. F. Weisskopf, *Phys. Rev. D* **9**, 3471 (1974); T. DeGrand, R. L. Jaffe, K. Johnson, and J. E. Kiskis, *Phys. Rev. D* **12**, 2060 (1975).
- [60] A. Breakstone *et al.*, *Z. Phys. C* **48**, 569 (1990).
- [61] E. Panagiotou, K. C. Millett, and S. Lambropoulou, *J. Phys. A* **43**, 045208 (2010); Claus Ernst *et al.* (unpublished).
- [62] D. Rolfsen, *Knots and Links* (Publish or Perish Inc., Berkeley, 1990).
- [63] L. H. Kauffman, *Knots and Physics* (World Scientific, Singapore, 2001).
- [64] E. Priest and T. Forbes, *Magnetic Reconnection: MHD Theory and Applications* (Cambridge University Press, Cambridge, 2000).
- [65] A. Casher, H. Neuberger, and S. Nussinov, *Phys. Rev. D* **20**, 179 (1979).
- [66] H. Neuberger, *Phys. Rev. D* **20**, 2936 (1979).
- [67] A. Casher, H. Neuberger, and S. Nussinov, *Phys. Rev. D* **21**, 1966 (1980).

- [68] For a discussion see T. Degrand and C. DeTar, *Lattice Methods for Quantum Chromodynamics* (World Scientific, Singapore, 2006), p. 96.
- [69] We note that attempts have been made to fit many of the  $f_J^{++}$  states into the quark model.
- [70] For a full discussion of these symmetries see M. Berglund *et al.*, *Symmetry* **4**, 143 (2012).
- [71] P. M. Bellan, *Spheromaks: A Practical Application of Magnetohydrodynamic Dynamos and Plasma Self-Organization*, (Imperial College Press, London, 2000).
- [72] See N. Oppermann, H. Junklewitz, G. Robbers, and T. A. Enßlin, [arXiv:1008.1246](https://arxiv.org/abs/1008.1246), and references therein.
- [73] A. F. Rañada, M. Soler, and J. L. Trueba, *Phys. Rev. E* **62**, 7181 (2000).
- [74] Y. M. Cho, *Int. J. Pure Appl. Phys.* **1**, 246 (2005); For recent work and a discussion of knotlike solutions in BECs and other systems, see Y. Kawaguchi, M. Nitta, and M. Ueda, *Phys. Rev. Lett.* **100**, 180403 (2008); *Phys. Rev. Lett.* **101**, 029902(E) (2008), and references therein. Older references can be found in [11].
- [75] R. V. Buniy and T. W. Kephart, *Int. J. Mod. Phys. A* **20**, 1252 (2005).
- [76] R. V. Buniy and T. W. Kephart, *Physical and Numerical Models in Knot Theory Including Applications to the Life Sciences*, edited by J. Calvo, K. C. Millett, E. J. Rawdon, and A. Stasiak, (World Scientific, Singapore, 2005), p. 45.
- [77] J. D. Bjorken, S. J. Brodsky, and A. S. Goldhaber, *Phys. Lett. B* **726**, 344 (2013).
- [78] V. Khachatryan *et al.* (CMS Collaboration), *J. High Energy Phys.* **09** (2010) 091.
- [79] D. Velicanu (CMS Collaboration), *J. Phys. G* **38**, 124051 (2011).
- [80] S. Todorova, *Phys. Rev. D* **86**, 034001 (2012).
- [81] S. Todorova-Nova, [arXiv:1309.6761](https://arxiv.org/abs/1309.6761).
- [82] B. Andersson, G. Gustafson, J. Hakkinen, M. Ringner, and P. Sutton, *J. High Energy Phys.* **09** (1998) 014.
- [83] M. Gell-Mann and Y. Ne'eman, *The Eightfold Way* (W. A. Benjamin Press, New York, 1964).
- [84] J. J. J. Kokkedee, *The Quark Model* (W. A. Benjamin Press, New York, 1969).
- [85] N. Isgur and J. E. Paton, *Phys. Lett.* **124B**, 247 (1983).
- [86] N. Isgur and J. E. Paton, *Phys. Rev. D* **31**, 2910 (1985).
- [87] E. Abreu and P. Bicudo, *J. Phys. G* **34**, 195 (2007).
- [88] G. S. Sharov, [arXiv:0712.4052](https://arxiv.org/abs/0712.4052).
- [89] S. Nussinov and R. Shrock, *Phys. Rev. D* **80**, 054003 (2009).
- [90] T. Barnes, *Z. Phys. C* **10**, 275 (1981).
- [91] J. M. Cornwall and A. Soni, *Phys. Lett.* **120B**, 431 (1983).
- [92] J. M. Cornwall and A. Soni, *Phys. Rev. D* **29**, 1424 (1984).
- [93] J. M. Cornwall and A. Soni, *Phys. Rev. D* **32**, 764 (1985).
- [94] W.-S. Hou, C.-S. Luo, and G.-G. Wong, *Phys. Rev. D* **64**, 014028 (2001).
- [95] W.-S. Hou and G.-G. Wong, *Phys. Rev. D* **67**, 034003 (2003).
- [96] S. Godfrey and N. Isgur, *Phys. Rev. D* **32**, 189 (1985).
- [97] S. Capstick, S. Godfrey, N. Isgur, and J. E. Paton, *Phys. Lett. B* **175**, 457 (1986).
- [98] D. LaCourse and M. G. Olsson, *Phys. Rev. D* **39**, 2751 (1989).
- [99] T. J. Allen and M. G. Olsson, *Phys. Rev. D* **68**, 054022 (2003).
- [100] F. Brau and C. Semay, *Phys. Rev. D* **70**, 014017 (2004).
- [101] D. Ebert, R. N. Faustov, and V. O. Galkin, *Phys. Rev. D* **79**, 114029 (2009).
- [102] F. Buisseret, *Phys. Rev. C* **76**, 025206 (2007).
- [103] A. Szczepaniak, E. S. Swanson, C.-R. Ji, and S. R. Cotanch, *Phys. Rev. Lett.* **76**, 2011 (1996).
- [104] A. P. Szczepaniak and E. S. Swanson, *Phys. Lett. B* **577**, 61 (2003).
- [105] N. Boulanger, F. Buisseret, V. Mathieu, and C. Semay, *Eur. Phys. J. A* **38**, 317 (2008).